A theoretical analysis of the optimal electrode thickness and porosity

Haverkort, J. W.

DOI
10.1016/j.electacta.2018.10.065

Publication date
2019

Document Version
Final published version

Published in
Electrochimica Acta

Electrochimica Acta 295 (2019) 846–860

Contents lists available at ScienceDirect

Electrochimica Acta

journal homepage: www.elsevier.com/locate/electacta

A theoretical analysis of the optimal electrode thickness and porosity

J.W. Haverkort

Process & Energy Department, Delft University of Technology, Leeghwaterstraat 39, 2628 CB, Delft, the Netherlands

ARTICLE INFO

Article history:
Received 25 May 2018
Received in revised form
4 October 2018
Accepted 11 October 2018
Available online 26 October 2018

Keywords:
Porous electrodes
Secondary current distribution
Electrode effectiveness factor
Optimization

ABSTRACT

Using electrodes or catalytic layers that are porous increases the reactive surface area but also the distance that ions and electrons have to travel. Thicker electrodes, through their larger surface area, reduce the activation overpotential but increase the ohmic losses. There will therefore be an electrode thickness for which the voltage losses are minimal, corresponding to a maximum energy efficiency. Simple approximate relations are derived here for the value of this optimal thickness, for both Tafel and linearised Butler-Volmer kinetics. We additionally optimise the power density of Galvanic cells, the capacity of battery electrodes, and the porosity of both particulate and foam-like electrodes. For this analysis we introduce an intuitive new definition of the electrode effectiveness factor. An accurate explicit current-voltage expression, including the transition from linear to Tafel kinetics and from a single to a doubled Tafel slope, is obtained. The present analysis is limited to a configuration where ions and electrons enter and leave at opposite sides of the electrode, as in most stacks, and applies only when mass transfer effects can be neglected. These results can nonetheless be useful for optimization of various electrochemical devices including fuel cells, batteries, flow batteries, electrochemical reactors, and electrolysers.

1. Introduction

The most important characteristic of any electrochemical device is its relationship between cell potential and current. From the steady-state polarization curve, for example, the energy efficiency, maximum power density, and limiting current can be obtained. Great improvement in understanding of the polarization curve was obtained after the work of Ref. [60] in the context of corrosion processes. Useful analytical polarization equations for non-porous electrodes are, for example, provided by the semi-empirical model of Ref. [14] and the popular empirical correction for PEM (polymer electrolyte membrane or proton exchange membrane) fuel cells [36].

For commercial application the reactive surface area is usually enhanced using porous electrodes, sometimes referred to as three-dimensional or volumetric electrodes. These are typically made from metallic or carbon-based particles, solid foams, or from fibrous materials like cloths, mats, or paper containing catalytic coatings or dispersed catalytic particles. The potentials and current densities change over the thickness of such porous electrodes, requiring a more complex analysis. Newman and Tobias, in their seminal paper Ref. [49], considered both electronic and ionic losses as well as concentration polarization inside a porous electrode. Mass transfer limitations inside catalytic particles were later also included in so-called flooded-agglomerate models for gas-diffusion electrodes [25,53] or pseudo two-dimensional models (P2D) for lithium-ion batteries [16,23]. Pore models like those of Ref. [11] added significant understanding of the transient behaviour of porous electrodes, relevant for the important experimental techniques of cyclic voltammetry and electrochemical impedance spectroscopy [39].

In the present work we assume Ohm's law holds for both the ionic and the electronic current density. We do not include concentration effects like a spatially varying conductivity, a limiting current or concentration polarization. For the electrolyte this is a valid approximation when it has a high or unity transference number [7,15,17,47]. This holds for example in solid electrolytes like the ion exchange membranes used in various fuel cells and electrolysers [9,13,22,32,37,37,37,54]. Ohm's law also approximately holds when supporting electrolytes are used, as in various fuel cells [31,43], electrolysers [34,51] and (flow) batteries [3,33,56], or when the electroactive species concentration is high and well-mixed [26,29]. The concentration of a neutral reactant can often be assumed constant well below the limiting current and when the conversion per pass is low [1,2,42,44,68].

In section 2 we introduce the model assumptions, geometry, used notation, and the definitions and means to calculate the

E-mail address: J.W.Haverkort@tudelft.nl.

https://doi.org/10.1016/j.electacta.2018.10.065

Nomenclature

ΔV	Electrode overpotential $\Phi_{e^-}(x=L)-\Phi_{\text{ion}}(x=0)$ [V]
A	Projected electrode area [m^2]
a	Volumetric electroactive surface area [m^2 per m^3 of total volume]
b	Tafel slope $RT/\alpha F$ [V]
F	Faraday constant 96485.3329 [C/mol]
i	Current density [A/m^2]
i_*	Superficial exchange current density [A per m^2 of electroactive electrode area]
i_{2b}	Effective superficial exchange current density in double Tafel slope regime $\sqrt{i_*^{\text{tot}} i_{\frac{\sigma\kappa}{\sigma+\kappa}}/f}$ [A/m^2]
i_ς	Characteristic current density $b\varsigma/L$ [A/m^2]
i_*^{tot}	Total superficial exchange current density aLi_* [A/m^2]
L	Electrode thickness [m]
L_*	Characteristic length-scale i/ai_* [m]
L_ς	Characteristic length-scale $b\varsigma/i$ [m]
R	Ohmic resistance outside electrodes [Ω]
R_{ct}	Charge-transfer or activation resistance $\alpha b/i_*^{\text{tot}}A$ [Ω]
R_{eff}	Apparent resistance due to ineffectiveness [Ω]
R_{gas}	Gas constant 8.31446 [J/mol/K]
R_ς	Ohmic resistance $L/A\varsigma$ [Ω]
U	Open-circuit potential [V]
x	Coordinate through porous electrode, see Fig. 1 [m]

Dimensionless variables

$\overline{\eta}$	Surface overpotential η/b
$\overline{\kappa}$	Ionic conductivity $\kappa/(\sigma+\kappa)$
$\overline{\Phi}$	Potential Φ/b
$\overline{\sigma}$	Electronic conductivity $\sigma/(\sigma+\kappa)$
$\overline{x}$	Electrode coordinate x/L
$\bar{i}$	Electronic current density i_{e^-}/i_x
$\mathscr{E}$	Electrode effectiveness factor $1/(\vec{i}_0^{\overline{\sigma}}\vec{i}_1^{\overline{\kappa}})$ ($\mathscr{E}_{\text{lin}} = 1/(\overline{\sigma}\vec{i}_0+\overline{\kappa}\vec{i}_1)$)
$\mathscr{I}$	Electrode ineffectiveness factor $1/\mathscr{E}-1$ ($\mathscr{I}_{\text{lin}} = 1/\mathscr{E}_{\text{lin}}-1$)
f	The function $f(\lambda,\delta)\equiv\mathscr{I}/\delta$

Greek variables

α	Charge transfer coefficient [-]
δ	Inverse Wagner number $\delta_\sigma+\delta_\kappa = \frac{iL}{b}\left(\frac{1}{\sigma}+\frac{1}{\kappa}\right)$ [-]
δ_*	Dimensionless current density i/i_*^{tot} [-]
δ_ς	Inverse Wagner number $iL/b\varsigma$ [-]
ε	Volume fraction [m^3 per m^3 of electrode volume]
η	Surface overpotential $\Phi_{e^-}-\Phi_{\text{ion}}$ [V]
κ	Effective ionic conductivity [S/m]
λ	Conductivity ratio $\sigma/\kappa+\kappa/\sigma$ [-]
ν	Defined below Eq. (20) and in Eq. (21) [-]
Φ	Potential [V]
χ	Value of $\delta^{\text{opt}}_{\sqrt{2\sigma\kappa}}$, see Eq. (50) [-]
σ	Effective electronic conductivity [S/m]
ς	A conductivity [S/m]

Subscripts and other notation

$'$	Derivative $d/d\overline{x}$ with respect to $\overline{x}$
0, 1	At $\overline{x}=0$ or $\overline{x}=1$, respectively
$^-$	Dimensionless quantity
e^-	Electronic (electrode)
x	Vector component in the x-direction
ion	Ionic (electrolyte)
lin	Linear(ised) (kinetics)
opt	Optimised for energy efficiency

electrode overpotential and *electrode effectiveness factor*. [9,52,55] We added *electrode* here to distinguish it from the more commonly used effectiveness factor related to mass transport in catalyst particles or agglomerates. Besides linear kinetics, section 3 also considers linearised Butler-Volmer kinetics to derive an expression for the approximate optimal electrode thickness over the whole range of current densities.

The Tafel analysis of Ref. [49] resulted in an *implicit* polarization relationship. Since this requires a numerical root solver it is not easily amenable to analytical optimization. Section 4 provides a convenient *explicit* polarization relation for Tafel kinetics that is approximate but highly accurate. It is combined with the exact solution for the linear part of symmetric Butler-Volmer kinetics, to give a solution that is valid over the whole range of current densities. The Tafel relation is used to derive expressions for the electrode thickness that maximises the energy efficiency as well as the power density. Section 5 uses a reaction-zone model to find the most efficient battery electrode thickness and under additional assumptions the electrode thickness providing the highest capacity. Finally in section 6 the optimal porosity is considered, where a useful analytical limiting result is compared to the exact numerical result.

2. Model equations

2.1. Definitions and assumptions

We consider the one-dimensional geometry shown in Fig. 1. By conservation of charge, in steady-state, the sum of the electronic and ionic current densities is a constant $i_{e^-}+i_{\text{ion}}=i_x$. For the chosen coordinate system, these vector components of the current density in the x-direction, are negative. We assume Ohm's law holds for both the electronic potential Φ_{e^-} in the conducting matrix of the electrode and the ionic potential Φ_{ion} in the solution or polymer constituting the electrolyte

$$i_{e^-}=-\sigma\frac{d\Phi_{e^-}}{dx} \quad \text{and} \quad i_{\text{ion}}=-\kappa\frac{d\Phi_{\text{ion}}}{dx}. \tag{1}$$

We consider how the *effective* electronic and ionic conductivities σ and κ may depend on the electrode properties in section 6.

Referring to Fig. 1, the cell potential reads

$$V_{\text{cell}}=U\pm(ARi+\Delta V+\Delta V_c), \tag{2}$$

with a minus sign for a Galvanic cell and a plus sign for an electrolytic cell. Here U is the open-circuit potential, $i\equiv|i_x|$, A the geometrical or projected electrode area, and R the ohmic resistance due to both ionic losses incurred in between the electrodes and the electronic losses in the current collectors and other circuitry. The product AR is sometimes referred to as the area-specific resistance. The *energy efficiency* of a Galvanic cell and an electrolytic cell are given by V_{cell}/U and U/V_{cell}, respectively. In both cases the efficiency is maximised by minimizing the losses $RAi+\Delta V+\Delta V_c$.

The potential difference $\Phi_{e^-}(x=0)-\Phi_{\text{ion}}(x=L)$ over the working electrode, the *electrode overpotential* is given by

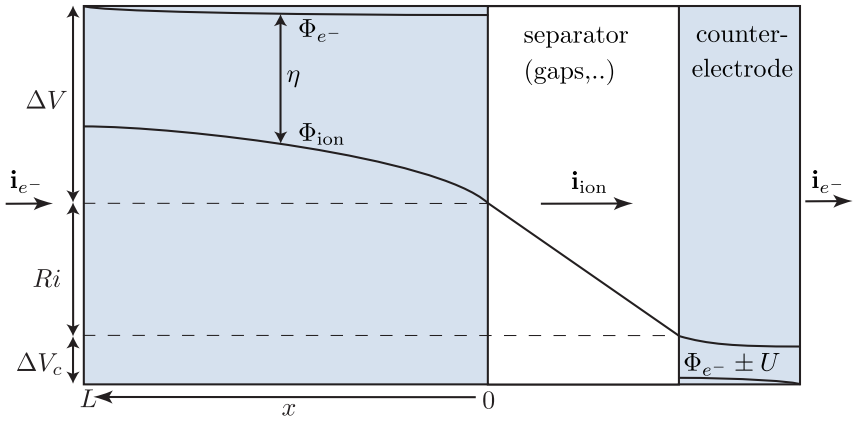

Fig. 1. A schematic illustration of the considered cell configuration, with the electroactive porous electrodes shaded. The ionic potential Φ_{ion} is measured relative to the (left) working electrode. For a cathodic working electrode the x-coordinate runs from left to right in the right electrode. The + and − sign on the bottom right refer to a Galvanic cell or electrolytic cell, respectively. The cell potential V_{cell} is given by the difference in potential between the left and right current-collectors.

$$\Delta V = |\eta(0)| + \Delta\Phi_{e^-} = |\eta(L)| + \Delta\Phi_{\text{ion}}, \tag{3}$$

where we use the notation $\Delta\Phi = |\Phi(L) - \Phi(0)|$. The *surface overpotential* $\eta \equiv \Phi_{e^-} - \Phi_{\text{ion}}$ is given by the difference between the electronic potential and the ionic potential measured, using the same material as the electrode, just outside the diffuse part of the electric double layer [47]. We thereby do not take into account the Frumkin correction due to diffuse charge effects [6]. We assume the reaction kinetics can be described by the Butler-Volmer equation. This gives the current density i_n normal to the surface of the pores inside the electrode, sometimes referred to as the transfer current density, as

$$i_n = i_*\left(e^{\eta/b} - e^{-\eta/b_c}\right). \tag{4}$$

Here i_* is the *superficial* exchange current density [A/m^2] and $b = R_{\text{gas}}T/\alpha F$ [V] the Tafel slope for the forward reaction under consideration, with α the corresponding charge transfer coefficient. For the backward reaction we write $b_c = R_{\text{gas}}T/\alpha_c F$. Here $\alpha + \alpha_c = 1$ and for a 'symmetrical' energy barrier $\alpha = \alpha_c = 1/2$ [5]. For the anodic working electrode considered in Fig. 1, the backward reaction is cathodic and the counter-electrode is the cathode. For a cathodic working electrode the subscript c should either be changed to a for anodic, or interpreted as referring to the counter-electrode and the 'complementary' backwards reaction. The ionic current density increases with increasing x according to

$$\frac{di_{\text{ion}}}{dx} = ai_n = ai_*\left(e^{\eta/b} - e^{-\eta/b_c}\right), \tag{5}$$

where ai_* is the *volumetric* exchange current density [A/m^3], with a the electrochemically active volumetric surface area [m^2 per m^3 of total electrode plus electrolyte volume] of the electrode.

2.2. Dimensionless notation

The ohmic potential drop due to a current density i traversing a length L of material with a conductivity ς is given by iL/ς. For Tafel kinetics, the ratio $b/(iL/\varsigma)$ is referred to as the Wagner number [47,66]. We will use the inverse

$$\delta_\varsigma \equiv \frac{iL}{b\varsigma}. \tag{6}$$

We can write $\delta_\varsigma = L/L_\varsigma = i/i_\varsigma = iAR_\varsigma/b$ in terms of a characteristic length-scale, current density, and area-specific resistance respectively, given by

$$L_\varsigma \equiv \frac{b\varsigma}{i},\quad i_\varsigma \equiv \frac{b\varsigma}{L},\quad AR_\varsigma \equiv \frac{L}{\varsigma}. \tag{7}$$

Here ς may for example be the ionic conductivity κ, giving δ_κ - referred to as ε in Ref. [49]. As in Ref. [49] and many later works, we define $\delta \equiv \delta_\kappa + \delta_\sigma$ which can be written in the form of Eq. (6) as $\delta = \delta_{\frac{\sigma\kappa}{\sigma+\kappa}}$ using the *series* circuit conductivity $\varsigma = 1/(1/\sigma + 1/\kappa) = \sigma\kappa/(\sigma + \kappa)$. We anticipate however that in a porous electrode the ionic and electronic current pathways are more similar to a *parallel* circuit governed by $\delta_{\sigma+\kappa}$.

We define

$$\delta_* \equiv \frac{i}{i_*^{\text{tot}}},\ \text{where } i_*^{\text{tot}} \equiv aLi_*. \tag{8}$$

Here i_*^{tot} is the total superficial exchange current density, obtained from i_* using the multiplication factor aL, sometimes referred to as the roughness factor, which represents the total internal surface area per geometrical electrode surface area. We note that in terms of the area-specific activation resistance or charge-transfer resistance $AR_{\text{ct}} \equiv \alpha b/i_*^{\text{tot}}$ we can write $\alpha\delta_* = iAR_{\text{ct}}/b$ so that $\alpha\delta_*$ is reminiscent of an inverse Wagner number. Contrary to δ_ς defined in Eq. (6) however, δ_* decreases with increasing electrode thickness L. Finally, we introduce the current density-dependent characteristic length-scale $L_* \equiv \alpha i/ai_*$ in terms of which we write $\delta_* = \alpha L_*/L$.

We will use $\overline{\sigma} \equiv \frac{\sigma}{\sigma+\kappa}$ and $\overline{\kappa} \equiv \frac{\kappa}{\sigma+\kappa}$, so $\overline{\sigma} + \overline{\kappa} = 1$, to denote the relative electronic and ionic conductivity, respectively. It will however also be useful to have a measure of the ratio of σ and κ that is symmetric in these conductivities. For this purpose we define $\lambda \equiv \frac{\sigma}{\kappa} + \frac{\kappa}{\sigma}$ in terms of which we can write

$$\lambda + 2 = \frac{(\sigma+\kappa)^2}{\sigma\kappa} = \frac{1}{\overline{\sigma}} + \frac{1}{\overline{\kappa}} = \frac{1}{\overline{\sigma}\,\overline{\kappa}} = \frac{\lambda}{\overline{\sigma}^2 + \overline{\kappa}^2}. \tag{9}$$

Here $\lambda + 2 = 1/\Omega$ or γ in the notation of Refs. [9] and [28], respectively. Note that $\lambda + 2 = (\sigma + \kappa)(1/\sigma + 1/\kappa)$ represents the ratio of the parallel and series conductivity and varies between 4 and infinity for $\sigma = \kappa$ and $\sigma/\kappa \to \infty$ or $\kappa/\sigma \to \infty$, respectively.

The following relations will also be useful in the analysis

$$\delta_{\sigma+\kappa} = \overline{\sigma}\delta_\sigma = \delta_\kappa\overline{\kappa} = \frac{\delta_\sigma\delta_\kappa}{\delta_\sigma+\delta_\kappa} = \frac{\delta}{\lambda+2} = \frac{\delta_{\sqrt{\sigma\kappa}}}{\sqrt{\lambda+2}}. \tag{10}$$

Following Ref. [49] we introduce a dimensionless coordinate $\overline{x}\equiv x/L$ and electronic current density $\bar{i}\equiv i_{e^-}(x)/i_x$ ranging from 0 where the ions enter, or leave in case of a cathode, to 1 at the position of the electronic connection. We define the dimensionless potentials $\overline{\Phi}_{e^-} = \pm\Phi_{e^-}/b$ and $\overline{\Phi}_{\rm ion} = \pm\Phi_{\rm ion}/b$ with a positive sign for an anodic working electrode and a negative sign for a cathodic working electrode. With this choice the dimensionless surface overpotential $\overline{\eta}\equiv\overline{\Phi}_{e^-} - \overline{\Phi}_{\rm ion}$ is always positive. Ohm's law, Eq. (1), can therefore be written in terms of only non-negative quantities as

$$\overline{\Phi}_{e^-} = \delta_\sigma\bar{i},\ \ \overline{\Phi}_{\rm ion} = \delta_\kappa\left(1-\bar{i}\right). \tag{11}$$

Here we use a prime to denote a derivative with respect to $\overline{x}$. The dimensionless electrode overpotential $\Delta\overline{V}\equiv\Delta V/b$, using Eq. (3), becomes

$$\Delta\overline{V} = \overline{\eta}_0 + \Delta\overline{\Phi}_{e^-} = \overline{\eta}_1 + \Delta\overline{\Phi}_{\rm ion}, \tag{12}$$

where we use a subscript 0 or 1 to denote the positions $\overline{x}=0$ and $\overline{x}=1$, respectively. We can write Eq. (5) as

$$\delta_*\bar{i}' = e^{\overline{\eta}} - e^{\frac{\alpha-1}{\alpha}\overline{\eta}}. \tag{13}$$

2.3. Electrode effectiveness factor

Adding $\overline{\sigma}$ times the first equality to $\overline{\kappa}$ times the second equality of Eq. (12) we obtain a more symmetric form

$$\Delta\overline{V} = \overline{\sigma}\overline{\eta}_0 + \overline{\kappa}\overline{\eta}_1 + \delta_{\sigma+\kappa}, \tag{14}$$

where used Eq. (11) and Eq. (10) to write $\overline{\sigma}\Delta\overline{\Phi}_{e^-} + \overline{\kappa}\Delta\overline{\Phi}_{\rm ion} = \delta_{\sigma+\kappa}$. The very useful Eq. (14) 'weighs' the surface activation overpotentials at $\overline{x}=0$ and 1 with the relative electronic and ionic conductivities $\overline{\sigma}$ and $\overline{\kappa}$, respectively. The dimensionless ohmic drop $\delta_{\sigma+\kappa}$ is that of a parallel circuit.

For sufficiently large surface overpotentials, the second exponential in Eq. (13) can be neglected compared to the first and we obtain the Tafel equation

$$\delta_*\bar{i}' \approx e^{\overline{\eta}}\ \ (\overline{\eta}\gtrsim 1). \tag{15}$$

Solving for the overpotential

$$\overline{\eta} = \ln\delta_*\bar{i}' = \ln\delta_* + \ln\bar{i}'. \tag{16}$$

Here the first term represents the activation overpotential, while the second term arises due to the inhomogeneity of the reaction. When the ionic conductivity is relatively low, the reaction can take place preferentially near $\overline{x}=0$ so that $\bar{i}'_0 \gg 1$ and $\bar{i}' \ll 1$ in the rest of the electrode.[1] This localization of the reaction increases the activation overpotential and causes the electrode to be used ineffectively. The characteristic length-scale $L/\bar{i}'_0$ is sometimes referred to as the 'penetration depth' [48,52] and the multiplier $1/\bar{i}'_0$ as the effectiveness factor [9,52,55]. It denotes the ratio of the current density to the current density $i_*^{\rm tot}e^{\overline{\eta}_0}$ that is obtained in the absence of resistivity. It was introduced initially for packed bed reactors. The same quantity is also often used in the fuel cells literature, see e.g. Refs. [35,57,67] where it is sometimes referred to as the (catalyst) utilization [50.] Ref. [65] considers a similar quantity $\left|\bar{i}'_0 - \bar{i}'_1\right|$, referring to this as the 'non-uniformity of the reaction rate'.

Equation (16) allows writing Eq. (14) as

$$\Delta\overline{V} = \ln\left(\frac{\delta_*}{\mathscr{E}}\right) + \delta_{\sigma+\kappa}, \tag{17}$$

where the *electrode effectiveness factor*

$$\mathscr{E} = \frac{1}{\bar{i}'^{\overline{\sigma}}_0\bar{i}'^{\overline{\kappa}}_1}. \tag{18}$$

This definition reduces to $1/\bar{i}'_0$ for $\sigma\gg\kappa$ but provides a natural generalization that is symmetric in σ and κ. The interpretation as the ratio of the current density to the current density in the absence of resistivity, is the same. We additionally introduce the *electrode ineffectiveness factor*

$$\mathscr{I}\equiv\frac{1}{\mathscr{E}} - 1 = \bar{i}'^{\overline{\sigma}}_0\bar{i}'^{\overline{\kappa}}_1 - 1, \tag{19}$$

which ranges between zero when $\mathscr{E}=1$ and infinity as $\mathscr{E}$ tends to zero.

3. Linearised kinetics

3.1. Linearised rate equation

For low overpotentials $\overline{\eta}\ll 1$, Eq. (13) can be accurately linearised around $\overline{\eta}=0$. For generality we introduce a linearisation around a value $\overline{\eta}_{\rm lin}$, giving

$$\bar{i}' \approx 1 + \frac{\nu^2}{\delta}(\eta - \eta_{\rm lin}), \tag{20}$$

where $\nu^2/\delta = \left(e^{\overline{\eta}_{\rm lin}} - \frac{\alpha-1}{\alpha}e^{\frac{\alpha-1}{\alpha}\overline{\eta}_{\rm lin}}\right)\Big/\delta_*$. We followed the suggestion of Ref. [49] to choose the value of $\bar{i}'$ for $\overline{\eta}=\overline{\eta}_{\rm lin}$ equal to the average reaction rate $\int_0^1 \bar{i}'\,d\overline{x} = 1$. Eq. (13) can in this case be solved exactly for $\overline{\eta}_{\rm lin}$ under the following limiting conditions

$$\overline{\eta}_{\rm lin} \approx \begin{cases} \alpha\delta_* \\ \ln\delta_* \\ \operatorname{asinh}\delta_*/2 \end{cases} \text{ and } \nu^2 \approx \begin{cases} \delta/\alpha\delta_* & (\delta_*\ll 1,\ \text{linear}) \\ \delta & (\delta_*\gg 1,\ \text{linearised Tafel}) \\ \delta\sqrt{1+(2/\delta_*)^2} & (\alpha=1/2,\ \text{linearised general}), \end{cases} \tag{21}$$

[1] Note from Eq. (16) that when $\bar{i}'\ll 1$ over part of the electrode, the Tafel approximation $\overline{\eta}\gtrsim 1$ requires $\delta_* = i/i_*^{\rm tot} \gg 1$ so that the current density should be large compared to the total superficial exchange current density $i_*^{\rm tot}$.

where we assumed α to be of order unity. In the linear case $\nu^2 = R_{\frac{\sigma\kappa}{\sigma+\kappa}}/R_{\mathrm{ct}}$ compares the series ohmic voltage to the voltage drop due to charge transfer, while in the Tafel case $\nu^2 = iR_{\frac{\sigma\kappa}{\sigma+\kappa}}/b$ this voltage is compared to the Tafel slope. The first and second limits of Eq. (21) are both considered in Ref. [49]. The final result will remain valid in the transition regime between linear and Tafel kinetics in case of equal charge transfer coefficients $\alpha = \alpha_c = 1/2$. For large values of its argument, $\operatorname{asinh}\frac{\delta_*}{2} \approx \ln\delta_*$ so that the middle and bottom limit of Eq. (21) agree in this case.

Combining Eqs. (20) and (21), the overpotential reads *for linearised kinetics*

$$\overline{\eta} \approx \begin{cases} \alpha\delta_*\bar{i}' & (\delta_* \ll 1) \\ \ln\delta_* + \bar{i}' - 1 & (\delta_* \gg 1) \\ \operatorname{asinh}\dfrac{\delta_*}{2} + \dfrac{\bar{i}' - 1}{\sqrt{1 + (2/\delta_*)^2}} & (\alpha = 1/2) \end{cases} \tag{22}$$

The middle expression may be contrasted with the Tafel expression of Eq. (16).

3.2. Linear electrode effectiveness factor

Inserting the limiting cases of Eq. (22) in Eq. (14) gives

$$\Delta\overline{V} \approx \delta_{\sigma+\kappa} + \begin{cases} \alpha\delta_*/\mathscr{E}_{\mathrm{lin}} & (\delta_* \ll 1) \\ \mathscr{I}_{\mathrm{lin}} + \ln\delta_* & (\delta_* \gg 1) \\ \dfrac{\mathscr{I}_{\mathrm{lin}}}{\sqrt{1 + (2/\delta_*)^2}} + \operatorname{asinh}\dfrac{\delta_*}{2} & (\alpha = 1/2) \end{cases}. \tag{23}$$

Here $\mathscr{I}_{\mathrm{lin}} \equiv 1/\mathscr{E}_{\mathrm{lin}} - 1$ and, the *linear electrode effectiveness factor*

$$\mathscr{E}_{\mathrm{lin}} = \frac{1}{\overline{\sigma}\bar{i}_0' + \overline{\kappa}\bar{i}_1'}, \tag{24}$$

acts as a multiplier of the exchange current density in case of linear kinetics. When $\sigma \gg \kappa$, Eq. (24) reduces to the form $\mathscr{E}_{\mathrm{lin}} \approx 1/\bar{i}_0'$ introduced in previous works. The factor $\mathscr{E}_{\mathrm{lin}}$ represents the ratio of the current density to the current density $i_*^{\mathrm{tot}}\Delta V/\alpha b$ obtained in the absence of resistivity. In the linearised Tafel case, the ineffectiveness factor $\mathscr{I}_{\mathrm{lin}}$ appears linearly, similar to a dimensionless resistive voltage. Alternatively we may write $\Delta\overline{V} \approx \delta_{\sigma+\kappa} + \ln(\delta_* e^{\mathscr{I}_{\mathrm{lin}}})$, showing that $e^{-\mathscr{I}_{\mathrm{lin}}}$ behaves as an effectiveness factor, multiplying the exchange current density, in this case. However, as we will see in section 4, this exponential form strongly underestimates the actual electrode effectiveness when $\mathscr{I}_{\mathrm{lin}}$ is not much smaller than one.

Inserting $\bar{i}_0'$ and $\bar{i}_1'$ from the exact analytical solution of the current distribution, Eq. (A.3), we obtain using Eq. (9)

$$\mathscr{E}_{\mathrm{lin}} = \frac{\lambda+2}{\lambda + 2/\cosh\nu}\frac{\tanh\nu}{\nu} \approx \begin{cases} \dfrac{\tanh\nu}{\nu} & \lambda \gg \dfrac{2}{\cosh\nu} \\ \dfrac{\lambda+2}{\lambda\nu} & \nu \gtrsim 2 \end{cases}. \tag{25}$$

The top approximation always holds when $\sigma \gg \kappa$ or $\kappa \gg \sigma$. It has the same form as the effectiveness factor used in heterogeneous catalysis, in which case ν is called the *Thiele modulus*. See for example Ref. [41]. This analogy was first explicitly mentioned for infinite electronic conductivity in Ref. [8]. For $\nu \lesssim 0.4$ we have $\mathscr{E}_{\mathrm{lin}} \approx 1$, which for linear kinetics requires $\delta = \alpha\nu^2\delta_*$ to be very small. In the opposite limit $\nu \gtrsim 2$, when $\lambda \gg 1$ we find $\mathscr{E}_{\mathrm{lin}} = 1/\nu$. When however $\lambda = 2$ we find in the same limit an electrode effectiveness $\mathscr{E}_{\mathrm{lin}} = 2/\nu$ that is twice as large. This is because for $\sigma = \kappa$ there will be two instead of one narrow reaction zones, one near $\overline{x} = 0$ and one near $\overline{x} = 1$.

3.3. Linear kinetics

In the linear regime we use Eqs. (23) and (25) with $\nu^2 = \delta/\alpha\delta_* = \frac{i_*^{\mathrm{tot}}L}{\alpha b}\left(\frac{1}{\sigma} + \frac{1}{\kappa}\right) = L^2/L_*L_{\frac{\sigma\kappa}{\sigma+\kappa}}$ to write

$$\Delta\overline{V} = \delta_{\sigma+\kappa}\left(1 + \frac{2 + \lambda\cosh\nu}{\nu\sinh(\nu)}\right). \tag{26}$$

The dimensionless parameter ν can thus be read as a dimensionless electrode thickness independent of the current density. Fig. 2 shows the dimensionless electrode overpotential - thickness relationship. For thin electrodes ($\nu \lesssim 1$) the activation overpotential is dominant, while for thick electrodes ($\nu \gg 1$) ohmic losses dominate the electrode overpotential. Equation (25) shows that for $\nu \gtrsim 2$ the linear electrode effectiveness factor $\mathscr{E}_{\mathrm{lin}}$ becomes proportional to $1/\nu$ so that the activation losses $\alpha\delta_*/\mathscr{E}_{\mathrm{lin}}$ become independent of the electrode thickness. At this point, the energy efficiency can no longer be improved by increasing the electrode thickness and the electrode overpotential only increase with increasing thickness due to increasing ohmic losses.

From Fig. 2, there will be an optimal value for $\nu \sim 2$ for which $\Delta\overline{V}$ is a minimum, so that the energy efficiency is a maximum. The optimal electrode thickness thus reads $L_{opt} = \nu_{\mathrm{opt}}\sqrt{L_*L_{\frac{\sigma\kappa}{\sigma+\kappa}}} \gg L_*$, or

$$L_{\mathrm{opt}} = \nu_{\mathrm{opt}}\sqrt{\frac{\alpha b}{ai^*}\frac{\sigma\kappa}{\sigma+\kappa}}. \tag{27}$$

The ohmic term in Eq. (23) increases linearly with increasing L, while for a hypothetical fully effective electrode with $\mathscr{E}_{\mathrm{lin}} = 1$ the activation overpotential is inversely proportional to L. In this case, the optimal electrode thickness, obtained by setting the derivative of $\Delta\overline{V}$ with respect to L to zero, reads $L = \sqrt{L_*L_{\sigma+\kappa}}$. Comparing with Eq. (27), we see that including the electrode effectiveness replaces the parallel conductivity $\sigma+\kappa$ with the series conductivity $(\sigma^{-1} + \kappa^{-1})^{-1}$. In a fully effective electrode, the conversion between ionic and electronic current can be distributed to minimise the ohmic potential drop as in the case of parallel resistances. For an optimally thick electrode, however, this conversion takes place preferentially near the edges of the electrode. While ohmic in appearance, the associated additional losses may however equally well be counted as increased activation losses due to the localization caused by ohmic resistance. This shows how these losses are intimately intertwined for an optimally thick electrode.

For $\nu \ll 1$, we expand Eq. (26) in ν to give to first order $\Delta\overline{V} \approx \delta_{\sigma+\kappa} + \alpha\delta_* + f\delta$, with $f = (\lambda - 1)/3(\lambda + 2)$. This may be written as $\Delta V = A\left(R_{\sigma+\kappa} + R_{\mathrm{ct}} + R_{\mathrm{eff}}\right)i$ where we define the area-specific ineffectiveness-related resistance

$$AR_{\mathrm{eff}} = \frac{L}{3}\frac{\lambda - 1}{\sigma + \kappa}. \tag{28}$$

Using Eq. (9) we obtain $AR_{\sigma+\kappa} + AR_{\mathrm{eff}} = AR_{\frac{\sigma\kappa}{\sigma+\kappa}}/3 = L(\sigma+\kappa)/3\sigma\kappa$. This result has previously been found for a macrohomogeneous model in, for example, Ref. [22]. In the field of electrochemical double-layer capacitors, or supercapacitors, this same resistance is

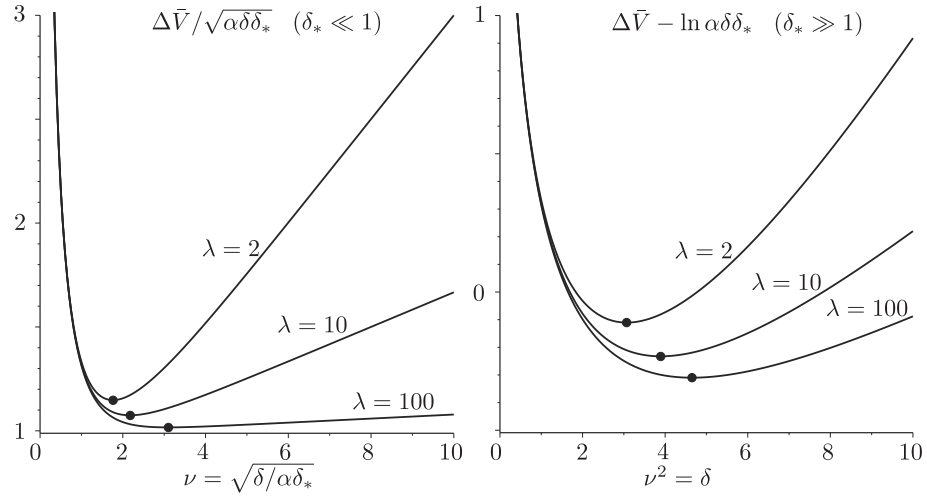

Fig. 2. The scaled dimensionless electrode overpotential for the case of linear kinetics (left) and linearised Tafel kinetics (right) as a function the dimensionless electrode thickness for different values of $\lambda = \sigma/\kappa + \kappa/\sigma$. The black circles indicate the position of the minimum and hence ν_{opt}. The ratio $\alpha\delta\delta_* = L_*/L_{\frac{\sigma\kappa}{\sigma+\kappa}}$ is independent of L.

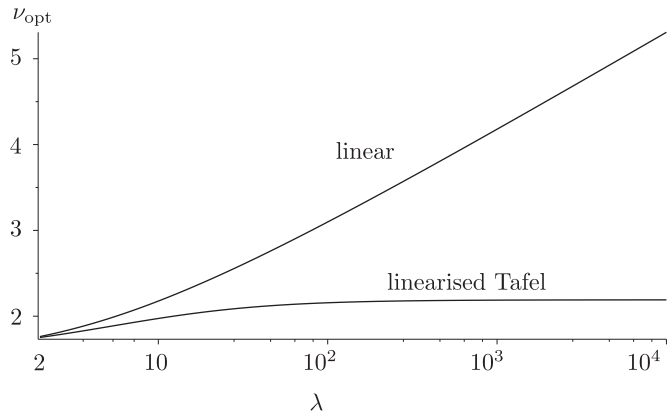

Fig. 3. The value of $\nu = \sqrt{\delta/\alpha\delta_*}$ in case of linear kinetics ($\delta_* \ll 1$) and $\nu = \sqrt{\delta}$ in case of linearised Tafel kinetics ($\delta_* \gg 1$) that minimises the linearised electrode overpotential $\Delta\bar{V}$ - as a function of $\lambda = \frac{\sigma}{\kappa} + \frac{\kappa}{\sigma}$.

referred to as the equivalent distributed resistance [24]. When $\sigma \gg \kappa$ this expression tends to $L/3\kappa$, which has been found, for example, in Ref. [61].[2] As mentioned in Ref. [50] this is in agreement with the result from a transmission line model [12].

Including electrode effectiveness, in this limit of $\nu \ll 1$, thus turns the parallel resistance $R_{\sigma+\kappa}$ into one-third of the series resistance, $R_{\frac{\sigma\kappa}{\sigma+\kappa}}/3$. For a homogeneously distributed reactivity, the area-specific resistance would be $L/2\sigma + L/2\kappa = AR_{\frac{\sigma\kappa}{\sigma+\kappa}}/2$. By the principle of minimum dissipation [22] the current distributes itself such that an optimum is found between reducing the activation losses and the ohmic losses.

For $\nu \geq 2$, Eq. (26) reads $\Delta\bar{V} \approx \delta_{\sigma+\kappa}(1 + \lambda/\nu)$. With $\nu^2 = R_{\frac{\sigma\kappa}{\sigma+\kappa}}/R_{ct}$ we write $\Delta V = AR_{\sigma+\kappa}i + \frac{\lambda}{\lambda+2}\sqrt{R_{\frac{\sigma\kappa}{\sigma+\kappa}}R_{ct}}Ai$. The final term can no longer be written as a sum of activation and resistive losses, illustrating their strong interaction.

Fig. 3 shows ν_{opt} as a function of λ, obtained by numerically minimizing Eq. (26). When $\lambda \gg 1$ we find analytically[3] $\nu_{opt} \approx \ln 2\sqrt{\lambda}$.

A good fit for all λ to the data shown in Fig. 3 is provided by

$$\nu_{opt} \approx \ln\left(2\sqrt{\lambda}\right)\left(1 + 1.24\Big/\lambda^{0.84}\right). \tag{29}$$

For $\nu_{opt} \gtrsim 2$ we can use $\delta^{opt}_{\sigma+\kappa} = \sqrt{\alpha\delta\delta_*}\nu_{opt}/(\lambda+2)$ to write

$$\Delta\bar{V}_{opt} \approx \sqrt{\alpha\delta\delta_*}\,\frac{\lambda + \nu_{opt}}{\lambda + 2}. \tag{30}$$

This simplified expression can be useful as a benchmark for the theoretically lowest possible electrode overpotential.

3.4. Linearised Tafel kinetics

For $\delta_* \gg 1$ we use Eqs. (23) and (25) with $\nu^2 = \delta = \delta_{\sigma+\kappa}(\lambda+2)$ to write

$$\Delta\bar{V} = \delta_{\sigma+\kappa}\left(1 + \frac{2 + \lambda\cosh\nu}{\nu\sinh\nu}\right) - 1 + \ln\delta_*. \tag{31}$$

Fig. 2 shows a rescaled $\Delta\bar{V}$ as a function of the dimensionless electrode thickness $\nu^2 = L/L_{\frac{\sigma\kappa}{\sigma+\kappa}}$. We see that again there is an optimal value $\nu_{opt} \approx 2$ so that

$$L_{opt} \approx \frac{\nu^2_{opt} b}{i}\,\frac{\sigma\kappa}{\sigma+\kappa}. \tag{32}$$

The optimal electrode thickness in this regime decreases with increasing current density i, which takes over the role of i^{tot}_* in Eq. (27) as a characteristic current density. Since the linearised Eq. (31) does not accurately take into account the electrode effectiveness in the Tafel regime, we have to await the full analysis of section 4 to see whether Eq. (32) accurately predicts the optimal electrode thickness.

Fig. 3 shows ν_{opt} as a function of λ, obtained by numerically minimizing Eq. (31). We see that ν_{opt} increases only slightly with λ and reaches a constant value $\nu_{opt} \approx 2.19$ when $\lambda \gg 1$. A good fit to the curve shown in Fig. 3 is provided by $\nu_{opt} \approx (2.19\lambda + 9.6)/(\lambda + 6)$.

3.5. Linearised general kinetics for $\alpha = 1/2$

In case of symmetric charge transfer coefficients $\alpha = \alpha_c$, the

[2] For equal ionic and electronic conductivity $\sigma = \kappa$ the area-specific resistance AR_{eff} is halved to $L/6\kappa$.

[3] Neglecting the $2/\nu\sinh$ term in Eq. (26) and setting the derivative with respect to ν to zero, gives $\tanh(\nu) = \sqrt{\lambda/(\lambda+1)} \approx 1 - 1/2\lambda$ so that $e^{2\nu} \approx 4\lambda$.

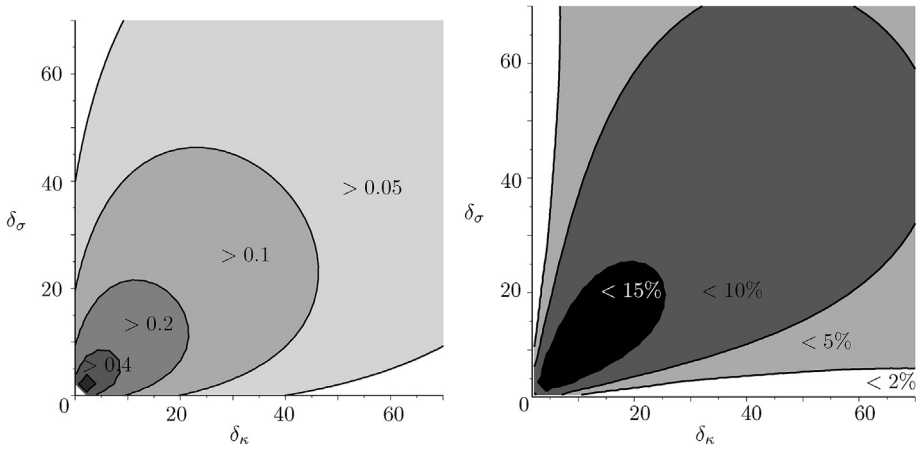

Fig. 4. The exact Tafel electrode effectiveness factor $\mathscr{E}$ (left) and the relative error in the approximation $\mathscr{E} \approx \left(1 + \frac{\lambda+1}{\lambda+10}\frac{\delta}{2}\right)^{-1}$ of Eq. (38) (right).

bottom result of Eq. (21) gives $\nu^2 = \delta\sqrt{1+(2/\delta_*)^2}$. Equating this to an optimal value ν^2_{opt} we find the optimal electrode thickness as

$$L_{\text{opt}} \approx \frac{L_*}{\sqrt{2}}\sqrt{\sqrt{1+\left(2\nu^2_{\text{opt}}\frac{L_{\frac{\sigma\kappa}{\sigma+\kappa}}}{L_*}\right)^2}-1} \approx \begin{cases} \nu_{\text{opt}}\sqrt{L_* L_{\frac{\sigma\kappa}{\sigma+\kappa}}} & (\delta_* \ll 1) \\ \nu^2_{\text{opt}} L_{\frac{\sigma\kappa}{\sigma+\kappa}} & (\delta_* \gg 1) \end{cases} \tag{33}$$

This general result reproduces the limiting cases of Eqs. (27) and (32) in case $\alpha = 1/2$ and provides an expression for intermediate values of δ_*. Fig. 3 shows that ν_{opt} will be similar in the linear and linearised Tafel regime for modest values of λ, so that in this case Eq. (33) is a useful approximation valid for all current densities.

4. Tafel kinetics

In most applications, the kinetics will be in the Tafel regime rather than the linear regime. There is an error associated with the linearisation used in the previous section. In this section we will reconsider the electrode overpotential, electrode effectiveness factor, and optimal electrode thickness without linearising. In A.2 we shortly revisit the original analysis of Ref. [49].

4.1. The Tafel electrode effectiveness factor

Contrary to the case of linearised kinetics we cannot obtain an exact explicit expression for the effectiveness factor for Tafel kinetics. Inserting the analytical expression of Eq. (A.8) in Eq. (19) gives with Eqs. (9) and (10)

$$\mathscr{E} = \frac{2}{\delta}\left(\overline{\sigma}^2 + \left(\frac{2\theta}{\delta}\right)^2\right)^{-\overline{\sigma}}\left(\overline{\kappa}^2 + \left(\frac{2\theta}{\delta}\right)^2\right)^{-\overline{\kappa}}. \tag{34}$$

Here θ has to be obtained from the following implicit equation

$$\theta\tan\theta = \frac{\delta}{2}\frac{(2\theta)^2}{(2\theta)^2 - \delta_\kappa\delta_\sigma}. \tag{35}$$

Since an explicit expression will be more useful and insightful we will seek an approximation that is accurate enough for further analysis. We may approximate $\tan\theta$ by $\theta/(1-\theta^2/3)$ which has the same first two terms in a Taylor expansion around $\theta = 0$. Solving Eq. (35) gives $(2\theta)^2 \approx (2\delta + \delta_\kappa\delta_\sigma)/(1+\delta/6)$, where $\delta_\sigma\delta_\kappa = \delta^2/(\lambda+2)$. With this expression, Eq. (34) approximates the exact effectiveness factor obtained numerically with a maximum error of less than 9%.

We can do even better by using $\tan\theta \approx \theta/(1-\theta^2/3-\theta^4/45)$ which captures the first *three* terms in an expansion around $\theta = 0$ exactly. Solving Eq. (35) with this approximation gives

$$(2\theta)^2 \approx \frac{6}{\delta}\left(\sqrt{\frac{10\delta^3}{\lambda+2}+45\delta^2+300\delta+900}-30-5\delta\right). \tag{36}$$

Using this in Eq. (34) gives the effectiveness factor with a maximum error around 3%. Inserted into Eq. (17) the cell voltage has an even smaller relative error, constituting a nearly exact solution. To investigate the solution for small δ we expand the resulting ineffectiveness factor $\mathscr{I} = 1/\mathscr{E} - 1$ in terms of δ. Both of the above approximations for θ, to first order in δ, give $\mathscr{I} = f\delta$ with

$$f_{\delta\to 0} = \frac{1}{3} - \overline{\sigma\kappa} = \frac{1}{3}\frac{\lambda-1}{\lambda+2}. \tag{37}$$

Since θ is bounded between zero and π, in the limit $\delta\to\infty$ Eq. (34) gives $\mathscr{I} = f\delta$, where now

$$f_{\delta\to\infty} = \frac{1}{2}\left(\overline{\sigma}^{\overline{\sigma}}\overline{\kappa}^{\overline{\kappa}}\right)^2 \approx \frac{1}{2}\frac{\lambda+1}{\lambda+10}. \tag{38}$$

The final simple rational approximation in terms of λ has the same limits for $\lambda = 2$ and $\lambda\to\infty$ and approximates the exact preceding result very well.[4]

An excellent fit to the numerical result for both $\lambda = 2$ and $\lambda \gg 1$ is obtained as

[4] Equation (38) gives $\mathscr{E} \approx 1/f\delta = 2/\delta$ for $\sigma \gg \kappa$ or $\kappa \gg \sigma$. When $\sigma = \kappa$ it gives $\mathscr{E} \approx 8/\delta$ so that the effectiveness seems to be four times higher. We should note however that δ for $\lambda = 2$ is twice that for $\lambda \gg 1$ so that the effectiveness really only doubles as is expected and in agreement with the linear case. Eq. (37) also gives the same doubling at $\lambda = 2$ compared to $\lambda \gg 1$. We note that the effectiveness generally increases as λ decreases. This implies that when e.g. $\sigma \gg \kappa$ the electrode effectiveness can actually be *improved* by *decreasing* the electronic conductivity. This goes however at the expense of increased ohmic losses, so that the total electrode overpotential increases.

$$f \approx f_{\delta\to 0} + \frac{f_{\delta\to\infty} - f_{\delta\to 0}}{1 + 3.28/\delta f_{\delta\to\infty}}. \tag{39}$$

The associated effectiveness factor

$$\mathscr{E} = (1 + f\delta)^{-1}, \tag{40}$$

has in these two cases a maximum error of less than 0.3%. This nearly-exact solution may be useful for example for validating numerical codes. For intermediary values of λ the behaviour of f requires the different functional form of Eq. (34) so that the maximum error is larger at about 7.5%.

Similar to what we did for linear kinetics in Eq. (28), we may write the overpotential $b\ln(1+\mathscr{I})$ associated with electrode ineffectiveness as $AR_{\text{eff}}i$, with $AR_{\text{eff}} = \frac{b}{i}\ln(1+f\delta)$.[5] When $f\delta \ll 1$ we obtain again Eq. (28) obtained in the linear case. For $\sigma \gg \kappa$ the resulting $AR_{\text{eff}} = L/3\kappa$ was previously derived from a macro-homogeneous model in Ref. [50], or from a transmission line model in, for example, Refs. [12,40]. This effective resistance approach however only holds in the limit of small δ. In general, a lowered effectiveness appears as an increased activation overpotential rather than an ohmic drop. As we have seen in the linear case and will soon derive for the Tafel case, the limit of small $\delta \ll 1$ in which the effectiveness factor is close to unity, is not necessarily the most optimal regime to be in from an energy efficiency perspective. When the electrode is so thin that it is fully utilised, the activation overpotential is unnecessarily high. In practice a typical PEM fuel cell catalyst layer, for example, primarily due to ionic resistance, has an electrode effectiveness much smaller than one [67].

If we do not mind that the limit $\delta \to 0$ is not captured exactly, the constant value $f_{\delta\to\infty}$ may be used. Fig. 4 compares Eq. (40) and the approximation in Eq. (38) with the exact numerical result. The largest error, for intermediate values of δ_σ and δ_κ, is with 14% acceptable for many purposes. An advantage of this very simple approximation is that f is in this case independent of δ, simplifying analytical optimization. When a higher accuracy is required Eq. (39) or Eq. (36) may be used.

4.2. Analytical current-voltage expressions

Inserting Eq. (40) in Eq. (17) gives

$$\Delta\overline{V} = \ln(\delta_*(1+f\delta)) + \delta_{\sigma+\kappa}, \tag{41}$$

or, re-introducing dimensions

$$\Delta V = b\ln\left(\frac{i}{aLi_*} + \frac{fi^2}{ai_*b}\frac{\sigma+\kappa}{\sigma\kappa}\right) + \frac{iL}{\sigma+\kappa}. \tag{42}$$

This simple explicit approximation to the exact Tafel kinetics electrode overpotential will be useful for further optimization from section 4.4 onward. First we will investigate the behaviour of this current-voltage curve in more detail.

When $\lambda \gg 1$, to a very high degree of accuracy $f \approx \frac{1}{3} + \frac{1/6}{1+2\cdot 3.28/\delta_\kappa}$ so that we obtain for $\sigma \gg \kappa$ the nearly exact result:

$$\Delta V \approx b\ln\left(\frac{i}{ai_*L}\left(1 + \frac{\delta_\kappa/2 + 6.56/3}{1 + 6.56/\delta_\kappa}\right)\right) + \frac{iL}{\sigma}. \tag{43}$$

[5] Amongst many others Refs. [50,58], considering PEM fuel cell cathodes, write this 'effective proton resistance' as $AR_{\text{eff}} = L(1/\sigma + 1/\kappa)/(3+\zeta)$, where the correction factor $\zeta = (\delta/\ln(1+f\delta)) - 3$ tends to zero for $\delta \to 0$.

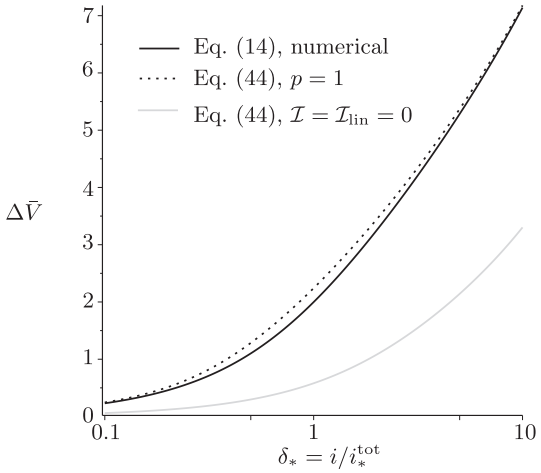

Fig. 5. A Tafel plot of the dimensionless electrode overpotential as a function of the dimensionless current density, for $\delta_\kappa = 10\delta_*$, $\delta_\sigma = 0.1\delta_*$, comparing the approximate analytical result of Eq. (44) using $p = 1$ to the numerical solution for symmetric Butler-Volmer kinetics (solving the boundary value-problem of Eqs. (11), (13) and (14) with $\alpha = 1/2$, $\bar{i}_0 = 0$ and $\bar{i}_1 = 1$). For δ_* much larger and smaller than one, respectively, Eq. (44) tends to Eq. (26) for linear kinetics and Eq. (43) for Tafel kinetics. Using instead $p = 2$ or $p = 1.75$ the analytical and numerical curves are largely indistinguishable. The grey solid line shows $\Delta\overline{V} = \text{asinh}\delta_*/2 + \delta_{\sigma+\kappa}$ for a fully effective electrode, showing the significance of accurately taking into account electrode effectiveness.

This equation clearly shows the transition from $f = 1/3$ for $\delta_\kappa \ll 1$ to $f = 1/2$ when $\delta_\kappa \gg 1$. When $\kappa \gg \sigma$ we can interchange σ and κ in this result.

The result of (41) can be matched to the exact linear kinetics solution of Eq. (26) in case of symmetric charge-transfer coefficients ($\alpha = \alpha_c = 1/2$) using, for a constant $p > 0$

$$\Delta\overline{V} \approx \text{asinh}\left(\frac{\delta_*}{2}\left(1 + \left(\mathscr{I}^p + \mathscr{I}_{\text{lin}}^p\right)^{1/p}\right)\right) + \delta_{\sigma+\kappa}. \tag{44}$$

Here $\mathscr{I} = f\delta$ where f is given approximately Eq. (38) or Eq. (39) and $\mathscr{I}_{\text{lin}} = 1/\mathscr{E}_{\text{lin}} - 1$ is obtained in exact form from Eq. (25). The Tafel regime requires $1/\delta_* \ll 1 + f\delta$ in which case $\mathscr{I}_{\text{lin}} \sim 1/\nu = \sqrt{\delta_*/2\delta} \ll f\delta$ and Eq. (44) tends to the Tafel result of Eq. (26). When on the other hand $1/\delta_* \gg 1 + f\delta$ we have $\mathscr{I}_{\text{lin}} \gg f\delta$ so that Eq. (44) tends to Eq. (26). Fig. 5 shows, for $p = 1$, a comparison of Eq. (44) with the numerical solution for symmetric Butler-Volmer kinetics. It can be seen that Eq. (26) indeed tends to the correct linear and Tafel kinetics limits. In between, the simple addition of ineffectiveness factors in Eq. (44) slightly overestimates the electrode overpotential. Using instead $p = 1.75$ keeps the error below 1% over the whole range of current densities. For smaller δ the lowest maximum error, typically well below 1%, is generally obtained using $p = 2$.

4.3. Tafel slope doubling

Equation (41) may be written as

$$\Delta\overline{V} = \ln\left(\frac{i}{i_*^{\text{tot}}} + \frac{i^2}{i_{2b}^2}\right) + \frac{i}{i_{\sigma+\kappa}}, \tag{45}$$

where $i_{2b}^2 = i_*^{\text{tot}} i_{\frac{\sigma\kappa}{\sigma+\kappa}}/f$. For low and high current densities, Eq. (45) is dominated by activation and ohmic losses, respectively, while for

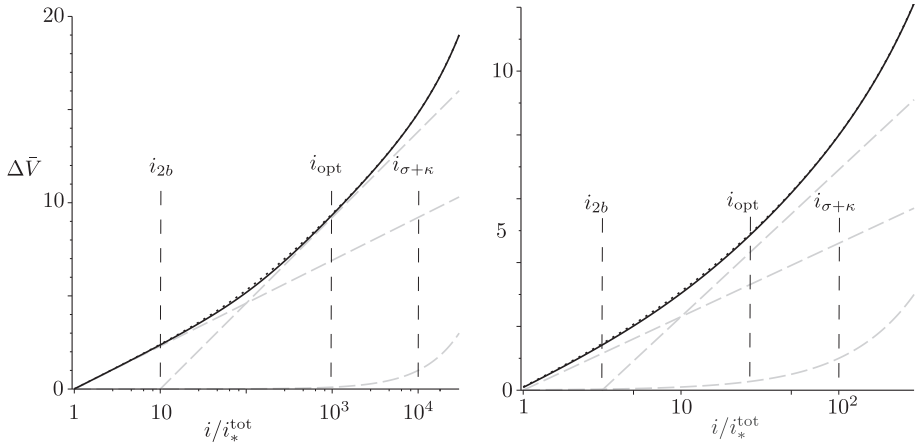

Fig. 6. A Tafel plot of the dimensionless electrode overpotential as a function of the dimensionless current density in case $\lambda \approx 207$ (left) and $\lambda \approx 25$ (right). The exact result (solid) and the approximation of Eq. (45) with f from (38) (dotted) largely overlap. The dashed lines indicate single and double Tafel slopes and the ohmic contribution $i/i_{\sigma+\kappa}$, respectively. The value of $i_{\rm opt}$ gives the current density for which the electrode overpotential is a minimum with respect to the electrode thickness.

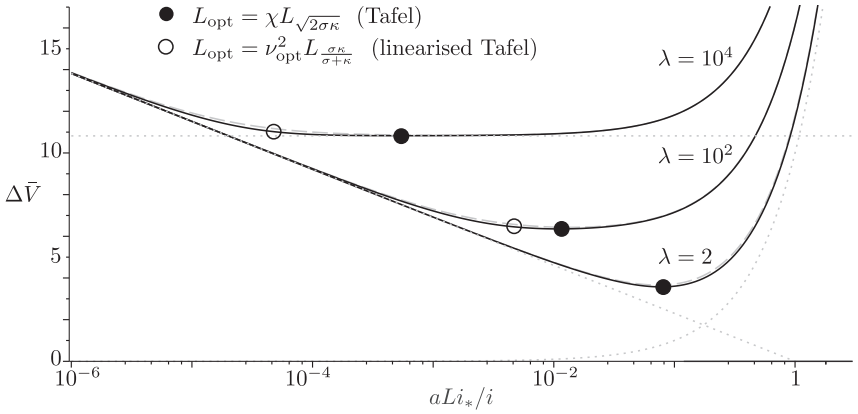

Fig. 7. The dimensionless electrode overpotential as a function of dimensionless electrode thickness $1/\delta_* = \delta_{\sigma+\kappa}/10$ (so the current density varies), for various values of $\lambda = \sigma/\kappa + \kappa/\sigma$. The exact result (solid) for most part overlaps the approximation of Eq. (49) with f from Eq. (38) (dashed). Also shown are $\ln\delta_*$, $\delta_{\sigma+\kappa}$ and $2\ln i/i_{2b}$ in case $\lambda = 10^4$ (dotted). The linearised Tafel optimum of Eq. (32) (empty circles) gives a nearly as low electrode overpotential as the exact optimum of Eq. (50) (solid circles) but with substantially smaller $L_{\rm opt}$, except for $\lambda = 2$ for which both overlap.

intermediate values the mixed losses $\Delta\bar{V} \approx 2\ln(i/i_{2b})$ dominate so that

$$i \approx i_{2b} e^{\Delta V/2b} \quad \left(i_{\frac{\sigma\kappa}{\sigma+\kappa}} \Big/ f \ll i \ll i_{\sigma+\kappa}\right), \tag{46}$$

In this regime we find a Tafel slope $\partial\Delta V/\partial\ln i = 2b$ of twice the usual value b. This 'Tafel-slope doubling' has been found theoretically and was experimentally verified many times in previous works [4,19,37,53,55,59]. When $\sigma \gg \kappa$, a measurement of the exchange current density in this regime would give an apparent value $i_{2b} \approx \sqrt{2i_*^{\rm tot} i_\kappa} = \sqrt{2ai_*\kappa b}$ in agreement with Ref. [4]. When $\kappa \gg \sigma$ the same expression results, with κ replaced by σ. Existence of the doubled Tafel-slope regime can be seen to require $\lambda \gg 1$, so that ohmic losses do not obscure its presence.

Fig. 6 shows Eq. (45) for two different values of λ, using for f the approximation of Eq. (38). The higher the value of λ, the clearer the Tafel slope doubling can be distinguished. Also the exact current-voltage curve is plotted, showing only a very small difference with Eq. (45). Using the more accurate Eq. (39) or Eq. (36) the difference would be still smaller.

From Eq. (17) we obtain the slope $\partial\Delta V/\partial\ln i = i\partial\Delta V/\partial i$ in a Tafel plot of ΔV versus $\ln i$ as

$$\frac{\partial\Delta V}{\partial\ln i} = b_{\rm eff} + AR_{\sigma+\kappa} i \tag{47}$$

where

$$b_{\rm eff} = b\left(1 + \mathscr{E}\delta\frac{d\mathscr{I}}{d\delta}\right) \approx b(2 - \mathscr{E}) \tag{48}$$

The final approximation follows from neglecting the weak dependence of f on δ which is a very good approximation.[6] Eq. (48) nicely shows the transition from a single Tafel slope b for $\mathscr{E} = 1$ to a double Tafel slope for $\mathscr{E} \ll 1$. This transition was considered numerically in for example Ref. [59]. Compensating for the ohmic drop in Eq. (47), this relation can be used to determine the effective Tafel slope $b_{\rm eff}$. Further compensating for effectiveness using Eq. (48), the true Tafel

[6] With $\mathscr{I} = f\delta$ we obtain $b_{\rm eff} = b(2 - \mathscr{E}(1 - \delta^2 df/d\delta))$ where, using Eq. (39) $\delta^2\frac{df}{d\delta} = 3.28(f_{\delta\to\infty} - f_{\delta\to 0})f_{\delta\to\infty}/(3.28 + \delta f_{\delta\to\infty})^2$. In the relevant limit $\lambda\to\infty$ this gives $(3.28/12)/(\delta/2 + 3.28)^2$ which is less than 0.05.

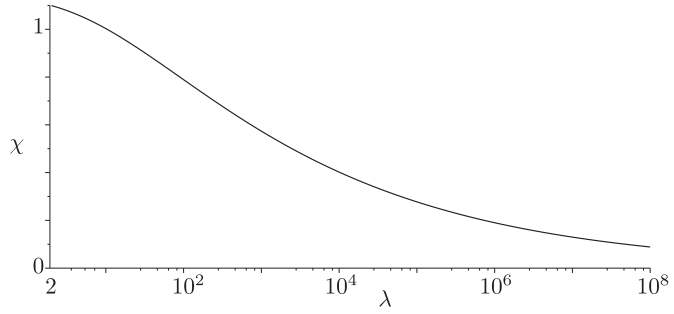

Fig. 8. The coefficient $\chi = L_{\rm opt}/L_{\sqrt{2\sigma\kappa}}$ as a function of $\lambda = \sigma/\kappa + \kappa/\sigma$ obtained from numerically minimizing the exact electrode overpotential. A good fit is provided by $\chi \approx \lambda^{0.36/(\ln\lambda)^{0.32}-0.274}$.

slope b and charge transfer coefficient $\alpha = R_{\rm gas}T/bF$ can be obtained.

Note that i_{2b}, and therefore the potential-current relationship (46), is independent of the electrode thickness L. The reason is that in this regime the effectiveness factor $\mathscr{E} \approx 2/\delta$ is inversely proportional to the electrode thickness so that increasing the electrode thickness merely reduces the electrode effectiveness, without changing the electrode overpotential. We therefore anticipate that the optimal electrode thickness will be somewhere in this regime. We will now proceed to derive an explicit relation for this thickness, which we already used in Fig. 6 to show the current density $i_{\rm opt}$ for which the electrode overpotential is minimised with respect to the electrode thickness.

4.4. Optimal electrode thickness

Eq. (41) may be written as

$$\Delta\overline{V} = \ln\left(\frac{L_*}{\alpha}\left(\frac{1}{L} + \frac{f}{L_{\frac{\sigma\kappa}{\sigma+\kappa}}}\right)\right) + \frac{L}{L_{\sigma+\kappa}}. \tag{49}$$

In Fig. 7 this is plotted as a function of the electrode thickness L for different values of λ using the approximation of Eq. (38) for f. Also the exact numerical result is shown, showing excellent agreement. The optimal electrode thickness that minimises the electrode overpotential of Eq. (49) can be obtained analytically as $L_{\rm opt} = \chi L_{\sqrt{2\sigma\kappa}}$[7] or (compare with Eq. (32))

$$L_{\rm opt} = \chi\frac{\sqrt{2\sigma\kappa}b}{i}, \tag{50}$$

with $\chi \approx 1$. Fig. 8 shows the result for χ obtained by numerically minimizing the exact electrode overpotential obtained from Eqs. (17), (34) and (35). For moderate values $\lambda \lesssim 10^2$ we see that $\chi \approx 1$ is a fair approximation. For large values of λ we see from Fig. 7 that there is a range of different electrode thicknesses with similar electrode overpotential. This corresponds to the double Tafel slope regime of Eq. (46). Therefore, other arguments like material costs or diffusion limitations of reactants, will often drive the practical optimum to smaller values than that predicted by Eq. (50). From Eq. (49) the 'plateau' of electrode thicknesses with similar electrode overpotential is given by

$$L_{\frac{\sigma\kappa}{\sigma+\kappa}}\Big/ f \lesssim L_{\rm opt} \lesssim L_{\sigma+\kappa}. \tag{51}$$

The optimum $L_{\rm opt} \approx 4L_{\frac{\sigma\kappa}{\sigma+\kappa}}$ of Eq. (32) predicted by the linearised Tafel analysis is at the lower part of this range and may therefore be a suitable value when a thinner electrode is desirable. For comparison, this optimal value is also shown in Fig. 7 and it can be seen to give only a slightly higher electrode overpotential than the exact minimum. When $\sigma \gg \kappa$, therefore, a sensible strategy is to choose an electrode thickness $\sim \kappa b/i$ using the lowest current density i for which a near optimal efficiency is desired. Up to current densities of the order of $i_{\sigma+\kappa} \sim (\sigma/\kappa)i$ the efficiency will then be near-optimal. To minimise the electrode or catalyst layer thickness, i here may also be the maximum attainable current density since the energy efficiency will be higher for lower current densities. For $\lambda = 2$, Eq. (50) and Eq. (32) predict almost exactly the same optimum. When σ and κ are of similar magnitude, as is clear from Fig. 7, near-maximum energy efficiency can be obtained only for a narrow range of current densities for a given electrode thickness.

Minimizing Eq. (17) with $\mathscr{E} = 1$ gives $L = L_{\sigma+\kappa}$. Compared with Eq. (50), including the electrode effectiveness factor changes the arithmetic mean conductivity $\frac{1}{2}(\sigma+\kappa)$ to the geometric mean conductivity $\sqrt{\sigma\kappa}$. This change implies that both σ and κ remain important even when one is much bigger than the other. By contrast, in the linearised Tafel optimum of Eq. (32) the series conductivity $\sigma\kappa/(\sigma+\kappa)$ appears so that the smallest conductivity determines the optimum: $L_{\rm opt} \approx 4L_\kappa$ for $\sigma \gg \kappa$ or $4L_\sigma$ for $\kappa \gg \sigma$.[8]

4.5. Optimally thick electrodes-examples

Inserting Eq. (50) into Eq. (49) gives the electrode overpotential of an optimally thick electrode as[9]

$$\Delta\overline{V}_{\rm opt} \approx 2\ln\left(\frac{i}{i_{2b}^{\rm opt}}\right) + \frac{\chi}{\sqrt{1+\lambda/2}}, \tag{52}$$

where $i_{2b}^{\rm opt} = \sqrt{ai_*\chi\sqrt{2\sigma\kappa}b/\mathscr{I}_{\rm opt}}$. Equation (52) holds only for the current density i used to calculate the optimum thickness. Using the fit[10] $\mathscr{I}_{\rm opt} \approx \chi\sqrt{0.34+\lambda/2}$, Eq. (52) may be useful as a benchmark for the lowest value of the electrode overpotential that is theoretically attainable in the Tafel regime. Note that the optimal electrode ineffectiveness increases without limit with increasing λ. Inserting instead the linearised Tafel result $\delta_{\rm opt} \approx 4$ of Eq. (32) in Eq. (40), gives $\mathscr{E} = 1/3$ when $\lambda \gg 1$ or $\mathscr{E} = 2/3$ in case $\lambda = 2$. Therefore, with this choice the electrode is used much more effectively while, as discussed in the previous section, the energy efficiency will be similar.

At this point it may be interesting to see what numerical values the optimal electrode thicknesses of Eqs. (32) and (50) predict for different applications. For a typical *flow battery* with a porous carbon electrode and liquid electrolyte, the effective conductivities σ and κ are of similar magnitude. With, say $\sigma = \kappa = 100$ S/m, $b =$

[7] Using Eq. (49) in $\partial\Delta\overline{V}/\partial L = 0$ gives, neglecting the very weak dependence of f on δ, $\chi = (\sqrt{1+4f(\lambda+2)}-1)/f\sqrt{8\lambda+16}$, which approximates to $\chi \approx 1/\sqrt{2f}$ for both $\lambda \gg 1$ and $\lambda = 2$ and always yields values close to 1 for intermediate values of λ. A more consistent notation would use the symbol $\delta^{\rm opt}_{\sqrt{2\sigma\kappa}}$ rather than χ.

[8] The semi-analytical approach of Ref. [45] assumed an exponential current distribution $1-\bar{i} = \exp(-x/L_{act})$ where $1/L_{act}$ minimises the corresponding electrode overpotential. The resulting expressions for the 'active thickness' L_{act} resemble but also differ from the optimal electrode thickness Eqs. (27), (32) and (50) more rigorously derived here.

[9] This shows why in Fig. 6 the current density $i_{\rm opt}$ is found approximately at the position where the slope $\partial\Delta\overline{V}/\partial\ln i = 2b$.

[10] The result $\mathscr{I}_{\rm opt} \approx 2f\chi\sqrt{1+\lambda/2}$, obtained by inserting $\delta_{\sqrt{2\sigma\kappa}} = \chi$ in Eq. (40), tends to the same result when $\lambda \gg 1$ but is less accurate for smaller values of λ.

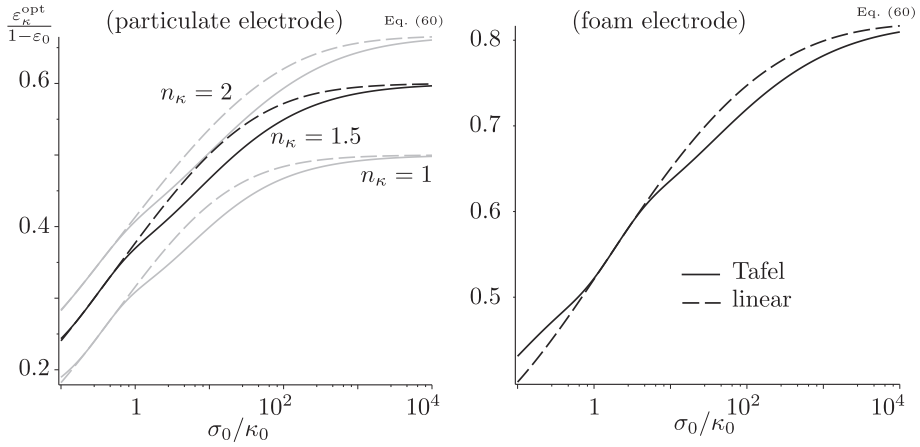

Fig. 9. The fraction, of the total volume fraction $1-\varepsilon_0$ that is available for either ionic or electronic conduction, that should be attributed to ionic conduction to maximise the energy efficiency of an electrode of optimal thickness, for Tafel kinetics (solid) and linear kinetics (dashed), as a function of the ratio of material electronic and ionic conductivities. In the limit $\sigma/\kappa\to\infty$ we may use Eq. (60), with $m_\sigma = 1$ and $m_\kappa = m_0 = 0$ for a particulate electrode (left) and $m_\sigma = 0.37$, $m_\kappa = 1$ for a foam-like electrode (right). For the foam-like electrode the differences between different values of $n_\kappa = n_\sigma$ is smaller than for a particulate electrode and therefore omitted for clarity.

50 mV, and $i = 0.3$ A/cm^2, both Eq. (50) and Eq. (32) give $L_{\rm opt}\approx 2.5$ mm. This is within the range typically employed and in agreement with the optimum of 2–3 mm reported in the hydrogen-bromine flow battery modeling study of Ref. [69]. We note from Fig. 7 that for $\lambda = 2$ there is a relatively narrow range of electrode thicknesses that give a near-optimal energy efficiency. Alternative, there is a relatively modest range of current densities for which a chosen electrode thickness gives near-optimal efficiency. Since in Ref. [69] an ionic and electronic conductivity of similar magnitude are used, an increased reactivity near the current collector as well as near the membrane was observed, similar to Fig. 10. A thinner optimum electrode thickness was found at a higher state-of-charge, which is explained by Eq. (32) since the ionic conductivity is lower in this case. A thinner optimum of 0.75 – 1 mm was also reported at a tenfold increased volumetric surface area. This can be explained by a transition towards linear kinetics. Using as a rough approximation the reported reference value $ai_* \approx 3\cdot 10^6$ A/m^3, $\kappa\approx 35$ S/m and $\nu_{\rm opt}\approx 2$, Eqs. (27) and (33) both give $L_{\rm opt}\sim 1$ mm.

By contrast, in *fuel cell* catalyst layers the ionic and electronic conductivities are very dissimilar. For a typical polymer electrolyte fuel cell, effective conductivities may be $\kappa = 1$ S/m and $\sigma = 10^4$ S/m so that with $b = 50$ mV and $i = 1$ A/cm^2, Eq. (32) gives $L_{\rm opt}\approx 24$ μm, within the range typically used, with, as just discussed, an effectiveness factor of $\mathscr{E}\approx 1/3$. For performing kinetic measurements a much higher effectiveness factor close to one is desirable [50] so that a much lower thickness has to be used. A much larger optimum thickness of $L_{\rm opt}\approx 300$ μm is predicted using Eq. (50) but the associated effectiveness factor of only $\mathscr{E}_{\rm opt}\approx 0.034$ indicates a very inefficient use of material. Also, at this thickness mass transport will dominate, invalidating this optimum. The top curve in Fig. 7 describes this case of $\lambda = 10^4$ and indicates the two different optimal thicknesses calculated here. The situation is similar in a typical solid oxide fuel cell and in many (water) *electrolysers*. Catalyst layers in fuel cells are typically several times smaller than the calculated optimum. From Fig. 7, in the considered example this would increases the electrode overpotential somewhat above its minimum. Reducing the electrode thickness for example by a factor four to 6 μm, as may be read off from Fig. 7 or calculated using the formulas of section 4.1, increases the electrode overpotential by less than a Tafel slope b, which may be acceptable. The effectiveness factor is increased to about 0.7 in this particular case. When made significantly thinner, however, the effectiveness becomes close to unity and no longer improves. In this case each halving of the electrode thickness increases the electrode overpotential by $b\ln(2)\approx 35$ mV, through increased activation losses. In some cases this may still be desirable to reduce the catalyst costs, especially when diffusion limitations further reduce the electrode effectiveness.

4.6. Maximum power density

For a *Voltaic or Galvanic cell*, like a battery or a fuel cell, an important parameter is the power density $P = iV_{\rm cell}$. The maximum power density is obtained at a current density $i_{\rm max}$ for which $\partial P/\partial i = 0$ so that $V_{\rm cell} = -\partial V_{\rm cell}/\partial \ln i$. The electrode thickness that maximises the power density is obtained by additionally requiring $\partial P/\partial L = -i\partial\Delta V/\partial L = 0$ which gives the same thickness as we obtained by maximizing the energy efficiency. In the previous section we found that for $\lambda\gg 1$ an optimally thick electrode is very ineffectively used so that Eq. (48) gives $\partial\Delta V/\partial\ln i\approx 2b$. With Eq. (2) we then find for a cell consisting of two such optimally thick electrodes *at maximum power*

$$V_{\rm cell} = 2b + 2b_c + ARi_{\rm max}. \tag{53}$$

Often the energy efficiency $V_{\rm cell}/U$ will be low in this case. Equation (2), (52), and (53) have to be solved for $i_{\rm max}$ numerically in general. In the limit of *negligible ohmic drop* $ARi_{\rm max}\ll 2b + 2b_c$

$$i_{\rm max} = i_{2b}^{\rm opt} e^{\frac{U-2(b+b_c)-\chi/\sqrt{1+\lambda/2}}{2(1+r)}} \tag{54}$$

when $\Delta V_c = r\Delta V$. In the opposite limit of negligible electrode overpotential $i_{\rm max}\approx U/2RA$. The maximum power density $P_{\rm max} = V_{\rm cell}i_{\rm max}$ is obtained by multiplying with Eq. (53).

5. Optimal battery electrode

In this section we will use the developed expressions to optimise the electrodes of a battery, using a reaction zone model similar to that of Ref. [63]. In batteries, typically the ionic conductivity is low enough that at a reasonable charge or discharge rate $\delta_\kappa\gg 1$. In this case, the reaction is localised in a thin reaction zone, or two if also $\delta_\sigma\gg 1$ as illustrated in Fig. 10 and for example Ref. [64]. We

assume that these reaction fronts move with a constant velocity, leaving behind fully discharged battery material with effective conductivities σ_d and κ_d that may differ from the initial values due to a change in material or porosity.

By charge conservation, the reaction fronts will be located at $\bar{x}_0 = \bar{\sigma}(1-\phi)$ and $\bar{x}_1 = 1-\bar{\kappa}(1-\phi)$, where ϕ is the state-of-charge (SOC).[11] The fully discharged regions give additional ohmic losses $iL\bar{x}_0/\kappa_d$ and $iL(1-\bar{x}_1)/\sigma_d$, respectively. The effective electrode thickness reduces over the discharge proportional to ϕ. Replacing L by ϕL in Eq. (49) and adding the additional ohmic losses, the electrode overpotential at a state of charge ϕ is given by

$$\Delta\bar{V}(\phi) = \ln\delta_* + \ln\left(\frac{1}{\phi}+f\delta\right) + (\phi+(1-\phi)\lambda_d)\delta_{\sigma+\kappa}, \tag{55}$$

where $\lambda_d \equiv \frac{\sigma}{\kappa_d}+\frac{\kappa}{\sigma_d}$ will equal λ when the effective conductivities before and after the discharge are equal. Eq. (55), together with Eq. (2), provides the battery voltage as a function of the state-of-charge. It may be compared with other generic battery models deployed in real-time battery management systems like Shepherd's, Unnewehr's or Nernst's model [27]. Or with the results from more comprehensive computational models as used in, for example, Refs. [10,18,20]. Although the present model contains more parameters, these all have a clear physical interpretation and can be obtained from independent experiments.

The average electrode overpotential over the discharge $\langle\Delta\bar{V}\rangle$ is obtained analytically by integrating Eq. (55) from the final state-of-charge ϕ_d to 1 and dividing by $1-\phi_d$. We obtain for a *deep discharge with* $\phi_d \ll 1$

$$\langle\Delta\bar{V}\rangle = \ln\delta_* + \ln(1+f\delta) + \frac{1+\lambda_d}{2}\delta_{\sigma+\kappa}. \tag{56}$$

This average voltage loss can be minimised for the electrode thickness by setting the derivative with respect to L to zero. This gives, neglecting the weak dependence of f on δ, an optimal value for δ or

$$L_{\text{opt}} \approx \delta_{\text{opt}}\frac{\kappa\sigma b}{i(\sigma+\kappa)}, \tag{57}$$

where $\delta_{\text{opt}} \sim \frac{1}{2f}\left(\sqrt{1+8f\frac{2+\lambda}{1+\lambda_d}}-1\right)$ and Eq. (38) gives $1/3 \le f \le 1/2$. When $\sigma \gg \kappa, \kappa_d$, Eq. (57) reads $L_{\text{opt}} \sim \delta_{\text{opt}}\kappa b/i$ with $\delta_{\text{opt}} \approx \sqrt{1+4\kappa/\kappa_d}-1$. Unless $\kappa_d \ll \kappa$ this solution does not generally satisfy the condition $\delta \gg 1$ used to derive Eq. (56). The real optimal value δ_{opt} may therefore be several times higher, at which point the assumption of thin reaction zones will be better satisfied. As an example we consider $\kappa = \kappa_d = 0.1$ S/m $\ll\sigma$, $b = 50$ mV, and $i = 10$ mA/cm^2 which gives $\delta_{opt} \approx 1.24$ and $L_{\text{opt}} \approx 62$ μm. Equation. (40) and (39) give for this case a quite high electrode effectiveness factor $\mathscr{E} \approx 0.7$ so that depletion of reactants occurs only near the end of the discharge. Therefore the additional ohmic losses due to fully discharged material included in Eq. (55) are absent over most of the discharge and the electrode can be made a few times thicker.

Often battery electrodes are sized to maximise the energy density or capacity rather than the energy efficiency. The total energy released is maximised when, at the end of a given discharge time, the battery reaches its minimum allowable voltage V_t [46]. Ideally, at this point the state-of-charge is small so that the battery material is used effectively, but not so small that the $1/\phi$ term in Eq. (55) dominates. Solving $V_{\text{cell}}(\phi_d) = V_t$ with Eq. (2) and Eq. (55) *assuming* $1 \gg \phi_d \gtrsim 1/f\delta \ll 1$ gives, with $\sigma \gg \kappa$[12]

$$L \approx \left(\frac{U-V_t-4b\ln(i/i_{2b})}{i} - RA\right)\frac{\kappa_d}{2}. \tag{58}$$

In the case of linear kinetics further simplification is possible, because the activation overpotential $\eta \lesssim b$ can usually be neglected. This optimization is done in, for example, in Refs. [46,63].

To obtain an even more general battery model we apply the same procedure used to derive Eq. (55) to Eq. (44) to obtain for symmetric Butler-Volmer kinetics

$$\Delta\bar{V}(\phi) = \operatorname{asinh}\left(\frac{\delta_*}{2}\left(\frac{1}{\phi}+\left(\mathscr{I}^p+\mathscr{I}_{\text{lin}}^p\right)^{\frac{1}{p}}\right)\right) + (\phi+(1-\phi)\lambda_d)\delta_{\sigma+\kappa}, \tag{59}$$

The assumption of thin reaction fronts requires $\delta, \nu \gg 1$ so that $\mathscr{I} = f_{\delta\to\infty}\delta$ and $\mathscr{I}_{\text{lin}} = \frac{\lambda\nu}{\lambda+2}-1$. In section 4.2 we found a value $p \approx 1.75-2$ to give the most accurate results. Integration gives for the average electrode overpotential during a deep discharge $\langle\Delta\bar{V}\rangle = \operatorname{asinh}\left(\frac{\delta_*}{2}(1+(\mathscr{I}^p+\mathscr{I}_{\text{lin}}^p)^{1/p})\right) + \frac{1+\lambda_d}{2}\delta_{\sigma+\kappa}$.

6. Optimal porosity

In this section we will investigate the optimal porosity of a flooded porous electrode. More generally, we investigate what fraction ε_κ of the electrode should ideally be used for ionic conduction and what fraction ε_σ for electronic conduction. Commonly, the dependence of the effective conductivity is taken into account through the Bruggeman correction factor: $\kappa = \kappa_0\varepsilon_\kappa^{n_\kappa}$ and $\sigma = \sigma_0\varepsilon_\sigma^{n_\sigma}$, with $n_\kappa \approx n_\sigma \approx 1.5$.[13] For generality we allow for a volume fraction ε_0 that conducts neither ions nor electrons, like a filler or binder. The fraction ε_0 can also represent a porosity for the transport of neutral species when, as for example in case of a solid electrolyte, these are not dissolved in the electrolyte. It then holds that $1 = \varepsilon_0+\varepsilon_\sigma+\varepsilon_\kappa$.

We will write the electrochemically active volumetric surface area as $a = a_0\varepsilon_\kappa^{m_\kappa}\varepsilon_\sigma^{m_\sigma}\varepsilon_0^{m_0}$. A monodisperse particulate electrode like a packed-bed electrode, pocket electrode, or sintered electrode is described by $m_\kappa = m_0 = 0$, $m_\sigma = 1$ and with a_0 the area to volume ratio of a single particle. For spherical particles of diameter d, for example, $a_0 = 6/d$. For solid-foams, the scaling of Ref. [30] can be accurately approximated using $m_0 = 0$, $m_\kappa = 1$, $m_\sigma = 0.37$. If not all of the surface area is electroactive, a multiplicative correction factor can be used.

We will now seek the optimal value for ε_κ that maximises the energy efficiency, assuming that the electrode thickness is also optimal in the same sense. When $\sigma \gg \kappa$, the final term in Eq. (52) is negligible so that minimizing the electrode overpotential amounts to maximizing $i_{2b,opt}^2 \approx 2ai_*\kappa b$. Solving $\partial(a\kappa)/\partial\varepsilon_\kappa = 0$ for ε_κ gives, using the above parametrizations

$$\frac{\varepsilon_\kappa^{\text{opt}}}{1-\varepsilon_0} = \frac{n_\kappa+m_\kappa}{n_\kappa+m_\kappa+m_\sigma} \quad \left(\frac{\kappa}{\sigma}\to 0,\ L = L_{\text{opt}}\right). \tag{60}$$

[11] With $Q_{\max}$ the maximum charge that can be extracted, the theoretical battery capacity, we have $\phi = 1-iAt/Q_{\max}$ after a time t. Often the C-rate is used in which C/h denotes a full theoretical discharge in h hours so that $i = Q_{\max}/3600Ah$.

[12] This assumes two electrodes with identical material properties. When instead the voltage of the counter-electrode is negligible we can replace $4b$ and $\kappa_d/2$ in Eq. (58) by $2b$ and κ_d, respectively. In general we have $L \approx (U-V_t-RAi-2(b\ln(i/i_{2b})+b_c\ln(i/i_{2b}^c)))/(\lambda_d/L_{\sigma+\kappa}+r\lambda_d^c/L_{\sigma+\kappa}^c)$ where $r = L^c/L$.

[13] Here κ_0 is the electrolyte ionic conductivity for $\varepsilon_\kappa = 1$, see however [62]. The factor $\varepsilon_\kappa^{n_\kappa} = \varepsilon_\kappa/\tau$, with τ the tortuosity. The exponents n_κ and $n_\kappa - 1$ are sometimes referred to as Archie's exponent and the Bruggeman exponent, respectively [38].

With $1-\varepsilon_0$ the volume fraction allowing either ionic or electronic conduction, the ratio $\varepsilon_\kappa^{\text{opt}}/(1-\varepsilon_0)$ gives the fraction of that volume which should ideally be attributed to ionic rather than electronic conduction. For a *particulate electrode*, with $m_\sigma = 1$ and $\varepsilon_0 = m_\kappa = m_0 = 0$, we obtain $\varepsilon_\kappa^{\text{opt}} = n_\kappa/(n_\kappa+1)$.[14] With the commonly used value $n_\kappa = 1.5$ this gives an optimal porosity of $\varepsilon_\kappa^{\text{opt}} = 0.6$.

For a *foam*-like electrode with $\varepsilon_0 = 0$, $m_\sigma = 0.37$ and $m_\kappa = 1$, we find a much higher value $\varepsilon_\kappa^{\text{opt}} = \frac{n_\kappa+1}{n_\kappa+1.37}$ which evaluates to 0.87 for $n_\kappa = 1.5$. The reason is that, while for a particulate electrode the surface area decreases with increasing ε_κ, for a foam electrode it increases up to relatively high values of ε_κ. Note that in these two examples the volumetric surface areas are similar but, due to the higher porosity, the ionic conductivity of the foam-like electrode is 1.8 times higher than that of the particulate electrode. This gives an electrode overpotential that, with $b \approx 50$ mV, is $b\ln 1.8 \approx 30$ mV lower.

Fig. 9 shows a comparison between the predicted optimal porosity ε_κ for a particulate and a foam-like electrode for a range of conductivity ratios. For linear kinetics, in the limit $\sigma \gg \kappa$, Eq. (30) gives $\Delta\overline{V}_{\text{opt}} \approx \sqrt{\alpha\delta_\kappa\delta_*}$. This expression is also minimised by maximizing $a\kappa$ so that Eq. (60) will again hold. Fig. 9 shows also the result from optimizing Eqs. (26) and (29) numerically.

In case of a solid electrolyte, part of the electrode volume has to be reserved for supply of reactants and products and possibly other functionalities. Deciding on the optimal value of the fraction ε_0 is beyond the scope of the present analysis. Since we did not include concentration effects, the present results only hold when mass transport does not provide significant limitations. For reactants dissolved in the electrolyte, this will hold at sufficient concentrations or when some advection is present as in the case of flow-through electrodes.

7. Conclusions

We studied theoretically the voltage losses of a porous electrode in which the ionic and electronic current enter and leave from opposite sides, as is common to most monopolar and bipolar stack configurations. This *electrode overpotential* is given by Eq. (14) in general or Eqs. (23) and (17) in case of linearised or Tafel kinetics, respectively. It consist of an ohmic drop featuring the parallel conductivity $\sigma + \kappa$, and an activation overpotential in which the exchange current density is multiplied by an *electrode effectiveness factor*. We provided simple definitions for this quantity, Eq. (18) and Eq. (24), valid for all ratios of ionic conductivity κ and electronic conductivity σ. For linear kinetics, an exact expression, Eq. (25), and for Tafel kinetics an approximate expression, Eq. (40), was found. With Eq. (39) this approximation is accurate to within 7% in general, or even 0.3% when σ and κ are either equal or very dissimilar. Alternatively, using Eqs. (34) and (36), the maximum error is around 3% for all values of σ and κ. The electrode effectiveness becomes inversely proportional to the electrode thickness so that the electrode overpotential start to increase beyond a certain optimal electrode thickness.

For Tafel kinetics, this optimal electrode thickness is given by $L_{\text{opt}} = \varsigma b/i$ so that at a given current density i the ohmic drop equals the Tafel slope b. Using $\varsigma \approx \sqrt{2\sigma\kappa}$, the theoretically lowest possible electrode overpotential is obtained. For very dissimilar σ and κ, however, the electrode is used very ineffectively with this choice. The linearised Tafel analysis resulting in Eq. (32), suggests using instead $\varsigma \approx 4\sigma\kappa/(\sigma+\kappa)$ which gives an almost as high energy efficiency, but results in thinner electrodes that use the electrode material more effectively. Finally, Eq. (57) suggests for a deeply discharged battery electrode a similar result. In this case additional ohmic losses due to fully discharged battery material lower the optimal electrode thickness. When a higher capacity is desired at the expense of a lower energy efficiency, useful state-of-charge dependent expressions for the overpotential are provided by Eqs. (59) and (55).

For linear kinetics, the total superficial exchange current density takes over the role of the current density i, resulting in the optimal thickness given by Eq. (27). Equation (33) provides an approximation for current densities in between the linear and Tafel regimes. Equation (44) provides a general explicit current-voltage relation for a porous electrode with symmetric Butler-Volmer kinetics that reduces to various exact limiting cases and typically has an error of less than 1%.

Finally we considered what volume fraction of a porous electrode should be used ideally for ionic conduction in case of negligible concentration polarization. The analytical expression of Eq. (60) for negligible electronic resistivity, predicts an optimal porosity of 0.6 for a particulate electrode and 0.87 for a typical foam-like electrode.

Appendix A. Analytical solutions for the current distribution

Appendix A.1 Linearised kinetics

Subtracting the second equality from the first in Eq. (11) gives

$$\overline{\eta}' = \delta\overline{i} - \delta_\kappa. \tag{A.1}$$

Taking the derivative of Eq. (20) with respect to $\overline{x}$ gives $\overline{i}'' = (\nu^2/\delta)\overline{\eta}'$. With Eq. (A.1) this gives

$$\overline{i}'' = \nu^2\left(\overline{i} - \overline{\sigma}\right). \tag{A.2}$$

The general solution to Eq. (A.2), with boundary conditions $\overline{i}_0 = 0$ and $\overline{i}_1 = 1$ is given by Refs. [21,47,49].

$$\overline{i} = \frac{\overline{\sigma}(\sinh\nu - \sinh\nu(1-\overline{x})) + \overline{\kappa}\sinh\nu\overline{x}}{\sinh\nu} \text{ and}$$
$$\overline{i}' = \nu\left(\frac{\overline{\sigma}\cosh(\nu(1-\overline{x})) + \overline{\kappa}\cosh(\nu\overline{x})}{\sinh\nu}\right). \tag{A.3}$$

For $\overline{\sigma} = 1$ and $\nu \gg 1$ the solution reads $\overline{i} \approx 1 - e^{-\nu\overline{x}}$. In this case the ionic current decreases exponentially with an e-folding 'penetration depth' L/ν. The effectiveness factor is in this case given by $1/\overline{i}_0' = 1/\nu$. From Eq. (A.3) we obtain the electronic potential drop as $\Delta\overline{\Phi}_{e^-} = \delta_\sigma\int_0^1 \overline{i}\,d\overline{x} = \delta_{\sigma+\kappa} + \delta_\sigma(\overline{i}_1' - \overline{i}_0')/\nu^2$. Inserting this into Eq. (12) gives for the electrode overpotential

$$\Delta\overline{V} = \overline{\eta}_{\text{lin}} + \frac{\delta_\kappa\left(\overline{i}_0' - 1\right) + \delta_\sigma\left(\overline{i}_1' - 1\right)}{\nu^2} + \delta_{\sigma+\kappa}. \tag{A.4}$$

The same result is alternatively obtained using the second equality of Eq. (12) or, without any knowledge of the current distribution, inserting Eq. (20) in Eq. (14).

[14] This same result was also found for the porosity in Ref. [63], when maximizing the capacity of a battery. The capacity was taken to be proportional to $L\varepsilon_\sigma$. With the optimal thickness L proportional to κ this gave same result.

Appendix A.2 Tafel kinetics

Taking the derivative of Eq. (15) with respect to $\bar{x}$ gives, with Eq. (A.1):

$$\bar{i}'' = \bar{i}'\bar{\eta}' = \bar{i}'\left(\delta\bar{i}' - \delta_\kappa\right) \tag{A.5}$$

A first integration of Eq. (A.5) gives $\bar{i}' = \bar{i}'_0 + \frac{\delta}{2}\bar{i}^2 - \delta_\kappa\bar{i}$ so that the dimensionless reactivity at $\bar{x} = 1$ reads

$$\bar{i}'_1 = \bar{i}'_0 + \frac{\delta_\sigma - \delta_\kappa}{2}. \tag{A.6}$$

Ref. [49] first derived the analytical solution to Eq. (A.5), its derivative, and integral as

$$\delta\bar{i} = \delta_\kappa + 2\theta\tan(\theta\bar{x} - \psi), \quad \delta\bar{i}' = \frac{2\theta^2}{\cos(\theta\bar{x} - \psi)^2} \quad \text{and} \quad \delta\int_0^{\bar{x}}\bar{i}d\bar{x} = \delta_\kappa\bar{x} + \ln\left(\frac{\bar{i}'}{\bar{i}'_0}\right) \tag{A.7}$$

An example solution is shown in Fig. 10. Here $\bar{i}_0 = 0$ requires $\tan\psi = \frac{\delta_\kappa}{2\theta}$, and to satisfy $\bar{i}_1 = 1$ the coefficient $0 < \theta < \pi$ has to be obtained iteratively from Eq. (35). In case of an infinite electronic conductivity $\delta_\sigma = 0$ Eq. (35) gives $\theta\tan\theta = \delta_\kappa/2$ so that $\psi = \theta$. From the expression for $\delta\bar{i}'$ in Eq. (A.7) we derive, using $1/\cos(\psi)^2 = 1 + \tan(\psi)^2$ and Eq. (A.6),

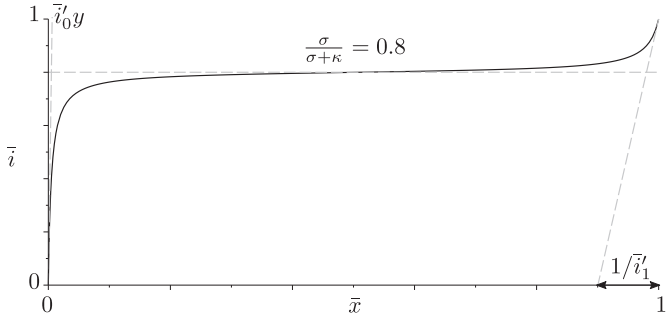

Fig. 10. The dimensionless electronic current density $\bar{i} = i_{e^-}/i_x$ for Tafel kinetics given by Eq. (A.7) for $\delta_\sigma = 100$ and $\delta_\kappa = 400$ so that $\delta = \delta_\sigma + \delta_\kappa = 500$. The ratio $\bar{\sigma} = \delta_\kappa/\delta = 0.8$ determines the current density in the bulk and the fraction of the current converted near $\bar{x} = 0$. Electrons involved in the reaction there have to travel over almost the entire electrode thickness. A fraction $\bar{\kappa} = 0.2$ of the ions travel approximately the entire electrode thickness to or from $\bar{x} \approx 1$. The slopes at $\bar{x} = 0$ and $\bar{x} = 1$ are given by Eq. (A.8) as $\bar{i}'_0 \approx \delta_\kappa^2/2\delta = 160$ and $\bar{i}'_1 \approx \delta_\sigma^2/2\delta = 10$ giving an electrode effectiveness factor $\mathscr{E} = 1/\bar{i}'_0\bar{i}'_1 \approx 1\%$. We note that for the Tafel approximation, Eq. (15), to remain valid over the entire domain requires $\bar{i}\delta_* \gtrsim 1$ for all $\bar{x}$.

$$\bar{i}'_0 = \frac{\delta_\kappa^2 + (2\theta)^2}{2\delta} \quad \text{and} \quad \bar{i}'_1 = \frac{\delta_\sigma^2 + (2\theta)^2}{2\delta}. \tag{A.8}$$

From Eq. (A.7), the electronic $\Delta\bar{\Phi}_{e^-} = \delta_\sigma\int_0^1\bar{i}d\bar{x}$ and ionic $\Delta\bar{\Phi}_{\text{ion}} = \delta_\kappa\int_0^1(1-\bar{i})d\bar{x}$ potential drops over the electrode read

$$\Delta\bar{\Phi}_{e^-} = \delta_{\sigma+\kappa} + \bar{\kappa}\ln\left(\frac{\bar{i}'_1}{\bar{i}'_0}\right) \quad \text{and} \quad \Delta\bar{\Phi}_{\text{ion}} = \delta_{\sigma+\kappa} - \bar{\sigma}\ln\left(\frac{\bar{i}'_1}{\bar{i}'_0}\right). \tag{A.9}$$

Inserting Eq. (A.9) into Eq. (12) gives for the dimensionless electrode overpotential Eq. (17), which we obtained without any knowledge of the current distribution using Eq. (14). See Ref. [48] for an overview of several publications deriving similar results in various limits. Also more recently several authors have re-derived the analytical solution of Eq. (A.7) for the case of an infinite electronic conductivity. See e.g. Refs. [19,50].

References

[1] Shahrir Abdullah, Siti Kartom Kamarudin, Umi Azmah Hasran, M.S. Masdar, Wan Ramli Wan Daud, Electrochemical kinetic and mass transfer model for direct ethanol alkaline fuel cell (deafc), J. Power Sources 320 (2016) 111–119.
[2] L. An, R. Chen, Mathematical modeling of direct formate fuel cells, Appl. Therm. Eng. 124 (2017) 232–240.
[3] Luis Fernando Arenas, F.C. Walsh, C. Ponce de León, The importance of cell geometry and electrolyte properties to the cell potential of zn-ce hybrid flow batteries, J. Electrochem. Soc. 163 (1) (2016) A5170–A5179.
[4] L.G. Austin, Tafel slopes for flooded diffusion electrodes, Trans. Faraday Soc. 60 (1964) 1319–1324.
[5] Allen J. Bard, Larry R. Faulkner, Electrochemical Methods: Fundamentals and Applications, vol. 2, wiley, New York, 1980.
[6] P.M. Biesheuvel, M. Van Soestbergen, M.Z. Bazant, Imposed currents in galvanic cells, Electrochim. Acta 54 (21) (2009) 4857–4871.
[7] C.C. Boyer, R.G. Anthony, A.J. Appleby, Design equations for optimized pem fuel cell electrodes, J. Appl. Electrochem. 30 (7) (2000) 777–786.
[8] F. Coeuret, D. Hutin, A. Gaunand, Study of the effectiveness of fixed flow-through electrodes, J. Appl. Electrochem. 6 (5) (1976) 417–423.
[9] Paola Costamagna, Paolo Costa, Vincenzo Antonucci, Micro-modelling of solid oxide fuel cell electrodes, Electrochim. Acta 43 (3–4) (1998) 375–394.
[10] Timo Danner, Madhav Singh, Simon Hein, Jörg Kaiser, Horst Hahn, Arnulf Latz, Thick electrodes for li-ion batteries: a model based analysis, J. Power Sources 334 (2016) 191–201.
[11] Robert De Levie, On porous electrodes in electrolyte solutions: I. capacitance effects, Electrochim. Acta 8 (10) (1963) 751–780.
[12] Robert De Levie, Electrochemical response of porous and rough electrodes, Adv. Electrochem. Electrochem. Eng. 6 (1967) 329–397.
[13] Hao Deng, Jixin Chen, Kui Jiao, Xuri Huang, An analytical model for alkaline membrane direct methanol fuel cell, Int. J. Heat Mass Tran. 74 (2014) 376–390.
[14] A. Dick, J. Larminie, Fuel Cell Systems Explained, John Wiley & Sons Ltd., Chichester., 2003.
[15] Kyle M. Diederichsen, Eric J. McShane, Bryan D. McCloskey, Promising routes to a high li+ transference number electrolyte for lithium ion batteries, ACS Energy Lett. 2 (11) (2017) 2563–2575.
[16] Marc Doyle, Thomas F. Fuller, John Newman, Modeling of galvanostatic charge and discharge of the lithium/polymer/insertion cell, J. Electrochem. Soc. 140 (6) (1993) 1526–1533.
[17] Marc Doyle, Thomas F. Fuller, John Newman, The importance of the lithium ion transference number in lithium/polymer cells, Electrochim. Acta 39 (13) (1994) 2073–2081.
[18] Zhijia Du, David L. Wood, Claus Daniel, Sergiy Kalnaus, Jianlin Li, Understanding limiting factors in thick electrode performance as applied to high energy density li-ion batteries, J. Appl. Electrochem. 47 (3) (2017) 405–415.
[19] M. Eikerling, AAa Kornyshev, Modelling the performance of the cathode catalyst layer of polymer electrolyte fuel cells, J. Electroanal. Chem. 453 (1–2) (1998) 89–106.
[20] Simon V. Erhard, Patrick J. Osswald, Peter Keil, Eike Höffer, Manuel Haug, Andreas Noel, Jörn Wilhelm, Bernhard Rieger, Korbinian Schmidt, Stephan Kosch, et al., Simulation and measurement of the current density distribution in lithium-ion batteries by a multi-tab cell approach, J. Electrochem. Soc. 164 (1) (2017) A6324–A6333.
[21] J. Euler, W. Nonnenmacher, Stromverteilung in porösen elektroden, Electrochim. Acta 2 (4) (1960) 268–286.
[22] Yuriy Fedotov, Sergey Bredikhin, Continuum modeling of solid oxide fuel cell electrodes: introducing the minimum dissipation principle, J. Solid State Electrochem. 17 (7) (2013) 2049–2054.
[23] Thomas F. Fuller, Marc Doyle, John Newman, Simulation and optimization of the dual lithium ion insertion cell, J. Electrochem. Soc. 141 (1) (1994) 1–10.
[24] Thomas F. Fuller, John N. Harb, Electrochemical Engineering, John Wiley & Sons, 2018.
[25] J. Giner, C. Hunter, The mechanism of operation of the teflon-bonded gas diffusion electrode: a mathematical model, J. Electrochem. Soc. 116 (8) (1969) 1124–1130.
[26] Michael Gordon, Galen Suppes, Convection battery modeling, insight, and review, AIChE J. 59 (8) (2013) 2833–2842.

[27] Hongwen He, Rui Xiong, Hongqiang Guo, Shuchun Li, Comparison study on the battery models used for the energy management of batteries in electric vehicles, Energy Convers. Manag. 64 (2012) 113–121.
[28] Nathaniel C. Hoyt, S Wainright Jesse, Robert F. Savinell, Current density scaling in electrochemical flow capacitors, J. Electrochem. Soc. 162 (6) (2015) A1102–A1110.
[29] Brian Huskinson, Michael J. Aziz, Performance model of a regenerative hydrogen bromine fuel cell for grid-scale energy storage, Energy Sci. Technol. 5 (1) (2013) 01–16.
[30] Amer Inayat, Hannsjörg Freund, Thomas Zeiser, Wilhelm Schwieger, Determining the specific surface area of ceramic foams: the tetrakaidecahedra model revisited, Chem. Eng. Sci. 66 (6) (2011) 1179–1188.
[31] Ranga S. Jayashree, Michael Mitchell, Dilip Natarajan, Larry J. Markoski, Paul JA. Kenis, Microfluidic hydrogen fuel cell with a liquid electrolyte, Langmuir 23 (13) (2007) 6871–6874.
[32] Kui Jiao, Sen Huo, Zu Meng, Daokuan Jiao, Jixin Chen, Qing Du, An analytical model for hydrogen alkaline anion exchange membrane fuel cell, Int. J. Hydrogen Energy 40 (8) (2015) 3300–3312.
[33] Chi-Young Jung, Tae-Hyun Kim, Wha-Jung Kim, Sung-Chul Yi, Computational analysis of the zinc utilization in the primary zinc-air batteries, Energy 102 (2016) 694–704.
[34] Thomas Kadyk, David Bruce, Michael Eikerling, How to enhance gas removal from porous electrodes? Sci. Rep. 6 (2016) 38780.
[35] M. Kawase, K. Sato, R. Mitsui, H. Asonuma, M. Kageyama, K. Yamaguchi, G. Inoue, Electrochemical reaction engineering of polymer electrolyte fuel cell, AIChE J. 63 (1) (2017) 249–256.
[36] Junbom Kim, Seong-Min Lee, Supramaniam Srinivasan, Charles E. Chamberlin, Modeling of proton exchange membrane fuel cell performance with an empirical equation, J. Electrochem. Soc. 142 (8) (1995) 2670–2674.
[37] A.A. Kulikovsky, The regimes of catalyst layer operation in a fuel cell, Electrochim. Acta 55 (22) (2010) 6391–6401.
[38] Johannes Landesfeind, Johannes Hattendorff, Andreas Ehrl, Wolfgang A. Wall, Hubert A. Gasteiger, Tortuosity determination of battery electrodes and separators by impedance spectroscopy, J. Electrochem. Soc. 163 (7) (2016) A1373–A1387.
[39] Andrzej Lasia, Electrochemical Impedance Spectroscopy and its Applications, Springer, 2002.
[40] Mark C. Lefebvre, Rex B. Martin, Peter G. Pickup, Characterization of ionic conductivity profiles within proton exchange membrane fuel cell gas diffusion electrodes by impedance spectroscopy, Electrochem. Solid State Lett. 2 (6) (1999) 259–261.
[41] Octave Levenspiel, Chemical reaction engineering, Ind. Eng. Chem. Res. 38 (11) (1999) 4140–4143.
[42] Shingjiang Jessie Lue, Nai-Yuan Liu, Selvaraj Rajesh Kumar, Kevin Chi-Yang Tseng, Bo-Yan Wang, Chieh-Hsin Leung, Experimental and one-dimensional mathematical modeling of different operating parameters in direct formic acid fuel cells, Energies 10 (12) (2017) 1972.
[43] Jarosław Milewski, Gabriele Discepoli, Umberto Desideri, Modeling the performance of mcfc for various fuel and oxidant compositions, Int. J. Hydrogen Energy 39 (22) (2014) 11713–11721.
[44] Jarrod D. Milshtein, Kevin M. Tenny, John L. Barton, Javit Drake, Robert M. Darling, Fikile R Brushett, Quantifying mass transfer rates in redox flow batteries, J. Electrochem. Soc. 164 (11) (2017) E3265–E3275.
[45] Kosuke Miyawaki, Masashi Kishimoto, Hiroshi Iwai, Motohiro Saito, Hideo Yoshida, Comprehensive understanding of the active thickness in solid oxide fuel cell anodes using experimental, numerical and semi-analytical approach, J. Power Sources 267 (2014) 503–514.
[46] John Newman, Optimization of porosity and thickness of a battery electrode by means of a reaction-zone model, J. Electrochem. Soc. 142 (1) (1995) 97–101.
[47] John Newman, Karen E. Thomas-Alyea, Electrochemical Systems, John Wiley & Sons, 2012.
[48] John Newman, William Tiedemann, Porous-electrode theory with battery applications, AIChE J. 21 (1) (1975) 25–41.
[49] John S. Newman, Charles W. Tobias, Theoretical analysis of current distribution in porous electrodes, J. Electrochem. Soc. 109 (12) (1962) 1183–1191.
[50] K.C. Neyerlin, Wenbin Gu, Jorne Jacob, Alfred Clark, Hubert A. Gasteiger, Cathode catalyst utilization for the orr in a pemfc analytical model and experimental validation, J. Electrochem. Soc. 154 (2) (2007) B279–B287.
[51] Amin Nouri-Khorasani, Emile Tabu Ojong, Smolinka Tom, David P. Wilkinson, Model of oxygen bubbles and performance impact in the porous transport layer of pem water electrolysis cells, Int. J. Hydrogen Energy 42 (48) (2017) 28665–28680.
[52] M. Paulin, D. Hutin, F. Coeuret, Theoretical and experimental study of flow-through porous electrodes, J. Electrochem. Soc. 124 (2) (1977) 180–188.
[53] Mike L. Perry, John Newman, Elton J. Cairns, Mass transport in gas-diffusion electrodes: a diagnostic tool for fuel-cell cathodes, J. Electrochem. Soc. 145 (1) (1998) 5–15.
[54] Neal S. Rosenthal, Saurabh A. Vilekar, Ravindra Datta, A comprehensive yet comprehensible analytical model for the direct methanol fuel cell, J. Power Sources 206 (2012) 129–143.
[55] K. Scott, Short communication the effectiveness of particulate bed electrodes under activation control, Electrochim. Acta 27 (3) (1982) 447–451.
[56] A.A. Shah, R.S.R.W. Tangirala, R. Singh, R.G.A. Wills, F.C. Walsh, A dynamic unit cell model for the all-vanadium flow battery, J. Electrochem. Soc. 158 (6) (2011) A671–A677.
[57] Dongwoo Shin, Jin Hyun Nam, An effectiveness model for electrochemical reactions in electrodes of intermediate-temperature solid oxide fuel cells, Electrochim. Acta 171 (1–6) (2015).
[58] Udit N. Shrivastava, Kazuya Tajiri, Sources of current density distribution in the land-channel direction of a pemfc, J. Electrochem. Soc. 163 (9) (2016) F1072–F1083.
[59] Jeff N. Soderberg, Aislinn Anne C. Co, H.C. Sirk, Viola I. Birss, Impact of porous electrode properties on the electrochemical transfer coefficient, J. Phys. Chem. B 110 (2006) 10401–10410.
[60] Milton Stern, Al L. Geary, Electrochemical polarization i. a theoretical analysis of the shape of polarization curves, J. Electrochem. Soc. 104 (1) (1957) 56–63.
[61] Eric L. Thompson, Jorne Jacob, Wenbin Gu, Hubert A. Gasteiger, Pem fuel cell operation at- 20 c. ii. ice formation dynamics, current distribution, and voltage losses within electrodes, J. Electrochem. Soc. 155 (9) (2008) B887–B896.
[62] Indrajeet V. Thorat, David E. Stephenson, Nathan A. Zacharias, Karim Zaghib, John N. Harb, Dean R. Wheeler, Quantifying tortuosity in porous li-ion battery materials, J. Power Sources 188 (2) (2009) 592–600.
[63] William Tiedemann, John Newman, Maximum effective capacity in an ohmically limited porous electrode, J. Electrochem. Soc. 122 (11) (1975) 1482–1485.
[64] Ming Wang, Jianjun Li, Xiangming He, Han Wu, Chunrong Wan, The effect of local current density on electrode design for lithium-ion batteries, J. Power Sources 207 (2012) 127–133.
[65] Yun Wang, Xuhui Feng, Analysis of reaction rates in the cathode electrode of polymer electrolyte fuel cell i. single-layer electrodes, J. Electrochem. Soc. 155 (12) (2008) B1289–B1295.
[66] Alan C. West, Electrochemistry and Electrochemical Engineering: an Introduction, Columbia University, 2013.
[67] Zetao Xia, Qianpu Wang, Michael Eikerling, Zhongsheng Liu, Effectiveness factor of pt utilization in cathode catalyst layer of polymer electrolyte fuel cells, Can. J. Chem. 86 (7) (2008) 657–667.
[68] Dongjiang You, Huamin Zhang, Jian Chen, Theoretical analysis of the effects of operational and designed parameters on the performance of a flow-through porous electrode, J. Electroanal. Chem. 625 (2) (2009) 165–171.
[69] Xin You, Qiang Ye, Trung Van Nguyen, Ping Cheng, 2-d model of a h2/br2 flow battery with flow-through positive electrode, J. Electrochem. Soc. 163 (3) (2016) A447–A457.